MINISTRY OF EDUCATION
FEDERAL UNIVERSITY OF RIO GRANDE DO SUL
GRADUATE PROGRAM IN MECHANICAL ENGINEERING

SHAPE AND TOPOLOGY OPTIMIZATION OF COMPLIANT MECHANISMS ACTIVATED BY PIEZOCERAMICS

by

André Piva Romeu

A Dissertation for the degree of
Master in Engineering

Porto Alegre, September 2023

SHAPE AND TOPOLOGY OPTIMIZATION OF COMPLIANT MECHANISMS ACTIVATED BY PIEZOCERAMICS

by

André Piva Romeu
Mechanical Engineer

A Dissertation submitted to the committee of the Graduate Program in Mechanical Engineering (PROMEC), from the Engineering School of the Federal University of Rio Grande do Sul (UFRGS), as part of the necessary requirements to obtain the degree of

Master in Engineering

Field of Study: Solid Mechanics

Advisor: Prof. Dr. Daniel Milbrath De Leon
Co-Advisor: Dr. Juliano Fagundes Gonçalves

Evaluation Committee:

Prof. Dr. Alexandre Molter ..... PPGMMat / UFPEL

Prof. Dr. Felipe Tempel Stumpf ..... PROMEC / UFRGS

Prof. Dr. Ignacio Iturrioz ..... PROMEC / UFRGS

Prof. Dr. Felipe Roman Centeno
Coordinator of PROMEC

Porto Alegre, 12, 2023

Knowledge is no more expensive than ignorance,

and at least as satisfying

Michael Elliott

ACKNOWLEDGEMENTS

I would like to thank everyone in Gmap for the countless hours of support, especially my advisor, Dr. Daniel Milbrath De Leon, without you, this work wouldn't exist. To my colleagues, particularly Dr. Juliano Fagundes Gonçalves, for taking the time to answer any and all of my questions.

To my family for praising my education more than any. To Luiza, for seeing what was not there yet. To my friends for the welcome distractions and the acceptance of my absence. To Casey and Robert for accommodating my erratic time window and understanding that, sometimes, things take time. Thank you all for keeping the wolves from the door, in more ways than one.

Finally, I am very thankful for the financial support of the Coordenação de Aperfeiçoamento de Pessoal de Nível Superior (CAPES) and the Conselho Nacional de Desenvolvimento Científico e Tecnológico (CNPq), essential to the pursuit of knowledge in Brazil.

RESUMO

Esta dissertação tem como objetivo desenvolver um código e uma metodologia para a otimização topológica de materiais piezoelétricos no contexto de mecanismos flexíveis. Mecanismos flexíveis são dispositivos não rígidos e funcionam com a deformação do material para alcançar o objetivo proposto. Para sintetizar tais mecanismos, foi utilizada a otimização topológica. A otimização topológica é um método matemático que atribui uma quantidade prescrita de material a um domínio prescrito. A discretização do domínio pelo método dos elementos finitos é uma abordagem usual e o seu uso foi auxiliado pela utilização de bibliotecas Python gratuitas, como o projeto FEniCS (*Finite Element Computational Software*) e o *dolfin adjoint*. Entre o grande número de métodos para a otimização de topologia, o método PEMAP (*PiezoElectric MAterial with Penalization*) foi escolhido; um método semelhante ao SIMP(*Solid Isotropic Material with Penalization*), mas com o efeito piezoelétrico como um de seus fatores. Materiais piezoelétricos podem gerar campos elétricos a partir de deformações assim como ocorre o processo inverso com a aplicação de um campo elétrico. Atuadores piezoelétricos podem ser usados em diversas aplicações, dentre elas, sistemas de eletrônica embarcada e uso em equipamentos médicos, ambos necessitando aplicações em micro e nanoescala. Uma das características dos mecanismos flexíveis é a ausência de juntas e articulações, o que facilita o uso em pequenas escalas, uma vez que nenhuma montagem é necessária e não há folgas entre os componentes. A otimização topologica utilizada teve como objetivo a minimização de *mean compliance* e a maximização de *mean transduction*. Com a metodologia descrita neste trabalho, foram resolvidos cinco problemas de otimização dupla multi-objetiva de material piezoelétrico e não piezoelétrico com polaridade no plano estudado. Os resultados apresentados foram discutidos e a validação foi realizada com todos os passos anteriores do problema.

Palavras-chave: Mecanismos flexíveis; Otimização topológica; Material piezoelétrico

ABSTRACT

This dissertation aims to develop code and methodology for the topological optimization of piezoelectric materials in the context of flexible mechanisms. Flexible mechanisms are non-rigid devices that operate by deforming the material to achieve the intended objective. To synthesize such mechanisms, topological optimization was employed. Topological optimization is a mathematical method that assigns a prescribed amount of material to a prescribed domain. The discretization of the domain using the finite element method is a common approach, and its use was assisted by the use of free Python libraries, such as the FEniCS (Finite Element Computational Software) project and dolfin adjoint. Among the numerous methods for topology optimization, the PEMAP (PiezoElectric MAterial with Penalization) method was chosen; a method similar to SIMP (Solid Isotropic Material with Penalization), but with the piezoelectric effect as one of its factors. Piezoelectric materials can generate electric fields from deformations, just as the reverse process occurs with the application of an electric field. Piezoelectric actuators can be used in various applications, including embedded electronics and medical equipment, both requiring applications at micro and nanoscales. One characteristic of flexible mechanisms is the absence of joints and articulations, which facilitates their use at small scales, as no assembly is required, and there are no clearances between components. The topological optimization used aimed to minimize mean compliance and maximize mean transduction. With the methodology described in this work, five double multi-objective optimization problems for piezoelectric and non-piezoelectric materials with polarity in the studied plane were solved. The presented results were discussed, and validation was performed for all previous steps of the problem.

Keywords: Compliant Mechanism; Topology optimization; Piezoelectric material

CONTENTS

LIST OF FIGURES

LIST OF TABLES

LIST OF ACRONYMS AND ABBREVIATIONS

AIEE	American Institute of Electrical Engineers
CAPES	*Coordenação de Aperfeiçoamento de Pessoal de Nível Superior*
CM	Compliant Mechanism
CNPq	*Conselho Nacional de Desenvolvimento Científico e Tecnológico*
ESO	Evolutionary Structural Optimization
FEM	Finite Element Method
FEniCS	Finite Element Computational Software
GMAp	*Grupo de Mecânica Aplicada*
HTF	Helmholtz-type Filter
IEEE	Institute of Electrical and Electronics Engineer
IRE	Institute of Radio Engineer
LSM	Level Set Method
MEMS	Microelectromechanical System
MMA	Method of Moving Asymptodes
NIST	National Institute of Standards and Technology
PDE	Partial Differential Equation
PEMAP	Piezoelectric Material with Penalization
PEMAP-P	Piezoelectric Material with Penalization and Polarization
PPGMMat	*Programa de Pós-Graduação em Modelagem Matemática*
PROMEC	*Programa de Pós-Graduação em Engenharia Mecânica*
PZT	Lead Zirconate Titanate
SHF	Smooth Heaviside Filter
SIMP	Solid Isotropic Material with Penalization
TO	Topology Optimization
UFPel	*Universidade Federal de Pelotas*
UFRGS	*Universidade Federal do Rio Grande do Sul*

LIST OF SYMBOLS

Latin Symbols

$\mathcal{U}$	Energy density, [J/m^3]
a_0	MMA input weight variable
a_i	MMA input weight variable
c_i	MMA input weight variable
d_i	MMA input weight variable
z	MMA auxiliary scalar variable
y_i	MMA auxiliary vector variable
A_n	Generic project variable
F	Forward model
E	Electric vector field, [V/m]
D	Electric displacement vector, [C/m^2]
S	Deformation tensor
c	Elasticity tensor, [Pa]
e	Piezoelectric tensor, [C/m^2]
Y	Elastic Modulus, [Pa]
r	Strength parameter
$\boldsymbol{n}$	Normal vector
$\mathcal{H}$	Electric enthalpy, [J]
$f(\cdot)$	Function of $\cdot$
m	Number of inequality constraints
n	Number of variables
$\boldsymbol{K}$	Rotation matrix
L_2	Mean transduction
L_3	Mean compliance
$\boldsymbol{R}$	Rotation tensor 2x2
$\boldsymbol{T}$	Rotation tensor 3x3
$\boldsymbol{t}$	Force vector, [N]
$\boldsymbol{u}$	Displacement vector, [m]
U	Trial function on a vector space

V	Maximum volume
u_{test}	Test function on a vector space
v_{test}	Test function on a scalar space
$\mathfrak{f}$	Volume fraction
w	Number of equality constraints
$f_0(\cdot)$	Object function
$g_i(\cdot)$	Inequality constraint functions
$h_j(\cdot)$	Equality constraint functions

Greek Symbols

α	Smoothed Heaviside Function slope variable
β	Smoothed Heaviside Function threshold variable
ϑ	Volume, [m^3]
η	Penalization value
σ	Mechanical stress tensor, [Pa]
Γ	Boundary
ε	Dielectric tensor (permittivity), [F/m]
ν	Poisson's coefficient
ρ	Pseudo density
θ	Angle between electric field and polarization, [rad]
Ω	Domain
φ	Trial function on a scalar space
ϕ	Electric potential, [V]
ψ	Angle of rotation in x-axis for a 3D tensor
χ	Pseudo density

Superscripts

$(\cdot)^S$	$\cdot$ in the absence of mechanical strain
$(\cdot)^E$	$\cdot$ in a constant electric field
$\bar{(\cdot)}$	Maximum allowed value of $\cdot$
$\dot{(\cdot)}$	Derivative with respect to time of $\cdot$
$\hat{(\cdot)}$	Helmholtz-type filtered variable
$\tilde{(\cdot)}$	Smoothed Heaviside filtered variable
$(\cdot)^T$	Transpose of $\cdot$

$\breve{(\cdot)}$	$\cdot$ after first rotation
$\acute{(\cdot)}$	$\cdot$ on a Plane strain problem
$\grave{(\cdot)}$	$\cdot$ after second rotation
$(\cdot)^{[n]}$	Matrix $n \times n$

Subscripts

$(\cdot)_{PZT}$	$\cdot$ referent to the piezoelectric material
$(\cdot)_{ISO}$	$\cdot$ referent to the isotropic material
$(\cdot)_i$	First order tensor
$(\cdot)_{ij}$	Second order tensor
$(\cdot)_{ijk}$	Third order tensor
$(\cdot)_{ijkl}$	Forth order tensor
$(\cdot)_p$	Second order tensor expressed in Voigt notation
$(\cdot)_{pq}$	Forth order tensor expressed in Voigt notation
$(\cdot)_{min}$	Small value of $\cdot$, a non zero amount for computational purposes
$(\cdot)_0$	Initial value
$\underline{(\cdot)}$	Minimum allowed value of $\cdot$
$(\cdot)_d$	Referent to the positive electric potential
$(\cdot)_o$	Referent to the objective function
$(\cdot)_\phi$	Referent to an electric potential of zero (grounded)
$(\cdot)_u$	Referent to prescribed displacement
$(\cdot)_t$	Referent to mechanical loads
$(\cdot)_\rho$	Referent to the pseudo density ρ
$(\cdot)_\chi$	Referent to the pseudo density χ
$(\cdot)_x$	x-axis component
$(\cdot)_y$	z-axis component

1 INTRODUCTION

The first mention of the piezoelectric effect was made by a French mineralogist in 1817 [Piefort, 2001] and in 1880 Curie and Curie made the first demonstration of the phenomenon. The piezoelectric effect is the ability that some materials have to generate an electric field in response to applied mechanical stress or, for the invert process, generate mechanical energy through an applied electric field. The latter, called the inverse piezoelectric effect, was first theorized and proved a year after Curie's first paper by Lippmann [apud Moheimani and Fleming, 2006].

A decade later, German physicist, Woldemar Voigt published the basic theory relating piezoelectricity to crystal symmetry as a result of the tensorial nature of the effect. His theory formed the basis for the mathematical equations standardized by The Institute of Radio Engineers (IRE) in 1949. Later, in 1963, the IRE merged with the American Institute of Electrical Engineers (AIEE) forming The Institute of Electrical and Electronics Engineers(IEEE). The IEEE, in 1967, published the "Hamilton's Principle for Linear Piezoelectric Media" [Tiersten, 1967], consolidating the mathematics view on the linear piezoelectric effect.

Piezoelectricity started to have field applications with the development of sonars, during the First World War, where quartz ceramics were used to produce ultrasonic waves [Piefort, 2001]. During the years after the Great War, the most common applications for piezoelectric materials started development, such as microphones, accelerometers, and ultrasonic transducers.

One of the main drawbacks of piezoelectric materials is that the strain produced by the application of an electric field is very small. The most used piezoceramic, Lead Zirconate Titanate (PZT), has a recoverable linear strain of 0.1%. If the displacements produced by the inverse effect could be amplified, the set of possible applications for these materials could grow significantly. Following this idea, a compliant mechanism (CM) can be attached to the PZT in order to amplify the mechanism kinematics.

A compliant mechanism transmits force and motion through elastic deformation instead of hinges and gears. With the needless for distinct parts, CMs do not require lubricants and are usually frictionless [Howell, 2001]. CMs are generally composed of a single piece, making assembly and manufacturing easier. Highly scalable, the mechanisms

can work well with PZT's micro-scale applications. The compliant mechanism has inherent problems, mainly fatigue susceptibility, energy loss on deformation, and a difficult design methodology

At the end of the millenium, Salamon and Midha [1998] researched the mechanical advantages of compliant mechanisms, analyzing designs with concentrated and distributed compliance, which appeared in publications around the 1990s. While the concentrated compliance approach is, usually, easier to compare with the rigid solution, the mechanism's relationships between force and deflection are still difficult to be determined [Albanesi et al., 2010]. Moreover, this methodology requires a rigid mechanism design from the start, while dispersed compliance techniques are more general, with designs obtained without the need for any commitment or initial topological proposal. Disperse compliance designs can be created with the use of topology optimization techniques.

Topology optimization (TO) is a computational method that optimizes material distribution in a defined domain, minimizing a specified cost function to achieve the maximum performance for a system. Traditionally, the optimization minimizes material used and strain energy whilst maintaining mechanical strength [Bendsøe and Sigmund, 2004]. Compliant mechanisms, however, need to maximize the compliance of the system while adhering to some other constraint, usually a minimum amount of material or maximum stress. There are several distinct methods for topology optimization, among which the density-based method, the evolutionary structural optimization (ESO), and the level set method (LSM) are the most representative [Zhu et al., 2020].

One of the most widely-used methods for topology optimization is the density-based method developed by Bendsøe and Kikuchi [1988]. The Solid Isotropic Material with Penalization method is computationally efficient, robust, adjustable, easy to understand, and does not require homogenization of the microstructure [Rozvany and Olhoff, 2000]. The PEMAP method, developed by Silva and Kikuchi [1999] takes into account the multiphysics problem of piezoelectric effect when extending the SIMP method.

The density-based approach is usually solved using a Finite Element Method (FEM) iterative solution. There is an abundance of commercial and noncommercial solvers of differential equations, needed for computing an FEM problem, among them, is the FEniCS Project, a research and software project aimed at creating mathematical methods and software for automated computational mathematical modeling, with effi-

cient, and flexible software for solving partial differential equations (PDEs) using finite element methods [Alnæs et al., 2015]. The FEniCS Project is the open-source computing platform chosen for this work for its high-level programming language, Python and for solving the forward problem internally, without the need to code the FEM discretization.

The study of compliant mechanisms that incorporate piezoelectric materials is an area of active research with promising real-world applications in high-precision mechanisms. Such mechanisms can be found in a range of fields, including photographic machines and computer hard disks. The works of Sigmund et al. [1998] and Silva et al. [1999a] at the end of the millennium contributed to the notoriety of the subject. Although a great number of papers were published about topology optimization of piezoelectric material or compliant mechanisms, few managed to incorporate both (piezoelectricity and CM), and even fewer were able to optimize two materials as well. Within the studies that manage to integrate multimaterial and multi-physics optimizations, almost none uses the polarization and electric field in the plane being optimize, therefore restricted in the problem definition. With the rise of computer technology in recent years, the computational cost of solving finite element problems dwindles and a rise in topology optimization studies is clearly seen. The creation of free tools such as the FEniCS library, in 2003, helped the development of new research, such as Moscatelli's dissertation [2020] on soft actuator design using topology optimization method.

This dissertation aims to contribute to the study of compliant mechanisms with piezoelectric materials by presenting a methodology for topology optimization of those mechanisms. The method used, PEMAP, with the method of moving asymptotes (MMA) searches for the optimal arrangement of materials within a given space while taking into account the desired performance requirements. The two-stage optimization developed is capable of optimizing the piezoelectric topology, unlike most of the literature that chooses only one material to optimize.

1.1 Objectives

The main objective of this work is to propose a methodology to solve the multi-physics problem of topology optimization of a compliant mechanism with a piezoelectric material. To do so, a formulation using the concept of mean transduction and mean compliance will be tested. It is also a goal of the present work to develop and make

available a numerical code to implement the optimization of the piezoelectric material position and topology of the compliant mechanism.

In a more detailed manner, the specific objectives of this work are:

- propose a framework to deal with the optimization of the shape of the PZT and the topology optimization of the non-piezo part in order to amplify the output port displacement of the mechanism;
- test several configurations for boundary conditions and polarization profiles and obtain the designs that perform best for each case.
- develop a working code, using free software, with examples of the optimizations made using the workflow.

1.2 Outline of the work

This document begins with the current introductory chapter, contextualizing the work and showing its motivations and objectives. Following up the second chapter explores the development of the concepts through the literature in the section titled "Literature review". In "Theoretical background", the third chapter, mathematical equations are presented and explained, together with the theory used throughout the text, containing the constitutive equations of piezoelectric materials, theoretical explanations of compliant mechanisms, the SIMP and PEMAP methods of topology optimization, the filters used, and the MMA. Chapter 3 aims to clarify the core concepts.

The methodology implemented is presented in the fourth chapter, containing detailed information on the step-by-step of how to go about solving a piezoelectric topology optimization problem. Chapter five, the second to last, shows the results for all the benchmark tests done to validate the coding work as well as shows example cases and their results for the dual material optimization. Lastly, the Conclusion chapter. In it, the proposed idea is compared to the final result for deliberation on the topic at hand. Closing this dissertation, the bibliographic references are laid out.

2 LITERATURE REVIEW

2.1 Multi-material topology optimization

The integration of multiple materials within a structure has always been a challenge in the design of engineering systems subject to different physical requirements [Montemurro et al., 2023]. Multi-material design and topology optimization have been suggested as the leading method to reduce weight from conventional components and small assembly structures [Roper et al., 2018].

The first topology optimization problem of two different materials using the SIMP method was proposed by Sigmund and Torquato [1999]. They use a two-variable approach to create a three-phase structure (void, material one, and material two). Yin and Ananthasuresh [2001] developed the peak function interpolation technique, where, with only one variable, they were able to have a multi-material structure. Tanaka et al. [2003] published a study of multi-material optimization of adaptive stiffness design, using the multi-material to create the passive change in the stiffness according to the external loads. Two years later, Ren et al. [2005] studied the use of compliant mechanism topology optimization using two materials to increase the mechanical advantage of the device.

An optimization of multi-material to handle strength constraints based on material failure was presented by Ramani [2010]. In 2015, Park and Sutradhar presented a multi-resolution implementation for a 3D multi-material topology optimization problem. A year later, Zuo and Saitou published a paper on ordered multi-material SIMP, a continuation of Yin and Ananthasuresh's work, trying to solve the horizontal zero slope problem. Recently, the research done by Montemurro et al. [2023] on multi-material problems under inhomogeneous Neumann–Dirichlet boundary conditions clarified their role and influence on the topology optimization problem.

2.2 Topology optimization of compliant mechanisms

The design of compliant mechanisms is interesting partially because of its inherent multi-objective performance demand; on one hand, the compliant mechanism needs to suffice its mechanical functionalities with flexibility or displacement output, while, on the other hand, remaining stiff enough to sustain external loads or force output [Lin et al., 2008]

The use of the SIMP methodology to solve compliant mechanism optimizations was first introduced by Sigmund [1997]. A year later, Nishiwaki et al. [1998] used the concept of mean compliance to balance the requirements of both flexibility and minimizing strain energy. Lau et al. [2001] researched distinct ways of creating an objective function for compliant mechanisms and their benefits and shortcomings. In 2003, Saxena [Saxena and Saxena, 2003] published their work on honeycomb meshes and the benefit of no checkerboard problem they have. Lu and Chen [2010] studied the use of topology optimization for the manufacturing of a compliant mechanism of a prosthetic knee joint creating a bionic mechanism design using SIMP.

Leon et al. [2015] obtained hinge-free mechanisms using stress constraints applied to the optimization problem. Liu et al. [2017] studied the use of hyperelastic materials and the effects of large displacements on the topology optimization of complying mechanisms. Recently, in 2020, Leon et al. investigated the influence of a nonlinear formulation with a stress constraint, showing that it plays an important role in stress constrained problems. That same year, Zhu et al. reviewed topology optimization of compliant mechanisms, clearly showing increased research on the subject over the past three decades.

2.3 Topology optimization of piezoelectric materials

Actuators using the inverse piezoelectric effect have great properties, such as precision of movement and a backlash-free motion, in a microscale capacity [Mamiya, 2006]. They also play a key role in the development of microelectromechanical systems (MEMS), which are increasingly important in fields such as medicine, aerospace, and consumer electronics [Tai, 2012]. One of the major obstacles in using topology optimization for conventional structural design problems is the generation of complex geometries leading to high fabrication costs. However, this issue does not apply to the design of MEMS due to their distinct fabrication technology [Maute and Frangopol, 2003].

The piezoelectric optimization problem was first solved by the SIMP Method in 1998, with the works of Sigmund et al. and in the following years Sigmund and Torquato [1999] and Silva and Kikuchi [1999] worked on this problem, iterating new ideas and concepts. Kögl and Silva [2005] developed a methodology to optimize the distribution of materials and the polarity of the piezoelectric actuators. The topology optimization of compliant mechanisms using piezoelectric material evolved simultaneously with the opti-

mization of compliant mechanisms as a whole. With the works of Silva et al. [1999b] and Silva et al. [1999a], the framework of balancing mean transduction and mean compliance was developed. Sigmund [2001b,a] wrote a two-paper description of the topology optimization method applied to the design of multiphysics actuators and electro-thermomechanical systems.

The early 2000s saw a growth in research of piezoelectric materials in topology optimization, with papers by Silva et al. [2000]; Lau et al. [2000]; Carbonari et al. [2007]; Zheng et al. [2008]. The next decade saw Luo et al. [2010] use physical programming together with the SIMP method to capture the inherent multi-criteria characteristic of compliant actuators. Ruiz et al. [2013] optimize a piezoelectric sensor by optimizing the ground structure and the polarization profile of the piezoelectric layers. In 2016, Molter et al. researched topology optimization of static structures and piezoelectric actuators simultaneously, distributing both materials in the domain. Recently, Gonçalves et al. [2018] addressed the problem of piezoelectric actuator design for active structural vibration control, finding the optimum actuator layout and polarization profile simultaneously. He et al. [2021] work proposed a multi-material topology optimization approach for the design of energy-harvesting piezoelectric composite structures.

While the field of optimization of mechanisms using piezoelectric material is abundant, works that combine 2D mechanisms and piezoelectric actuation usually consider the polarization perpendicular to the plane, unlike the proposed in-plane polarization, which can lead to a more efficient mechanism.

3 THEORETICAL BACKGROUND

In this chapter, the necessary theory to understand this work is established. Firstly the theory of piezoelectricity and piezoelectric constitutive equations are shown, followed up by a brief explication of the SIMP method and its derivation, PEMAP. Sequentially, the filters used are mathematically described, and at the end of the chapter, the solving method for the optimization problem is expressed.

3.1 Piezoelectricity

Piezoelectricity is an electric charge that accumulates in some materials (crystals, ceramics, and biological matter) in response to applied mechanical stress [Piefort, 2001]. The piezoelectric effect is a reversible process, all materials that have it also exhibit the reverse piezoelectric effect, that is, the generation of mechanical strain resulting from an applied electric field.

Piezoceramics, such as PZT above a critical temperature, known as Curie temperature, exhibit a simple cubic symmetry without dipole moment -the separation of positive and negative electrical charges within. However, below the Curie temperature, each crystal of the piezoceramic material has tetragonal symmetry and, associated with it, a dipole moment. Adjacent dipoles create local alignment regions called dominions, each dominion has its own polarization angle, making the ceramic unpolarized on a macro scale [Gonçalves, 2015].

The dominions can be aligned through a process of polarization, just below the Curie temperature, where a strong and continuous electric field is prescribed onto the material. The electric field forces an alignment of all the dominions and with the removal of the electric field, most of the dipoles stay locked in a similar angle, creating a permanent polarization. The behavior of a polarized piezoelectric ceramic at a smaller temperature can be seen in Figure 3.1, where an electric potential difference is applied to a piezoceramic with different angles of polarization. The dashed square represents the original shape of the piezo before the current is applied, and the solid line indicates the displaced material.

For a perfect alignment of electric field and polarization, an angle θ of 0 radians, the material stretches along the normal and contract in the other axis, for the opposite, with $\theta = \pi$, the constriction happens along the normal and the elongation on the other

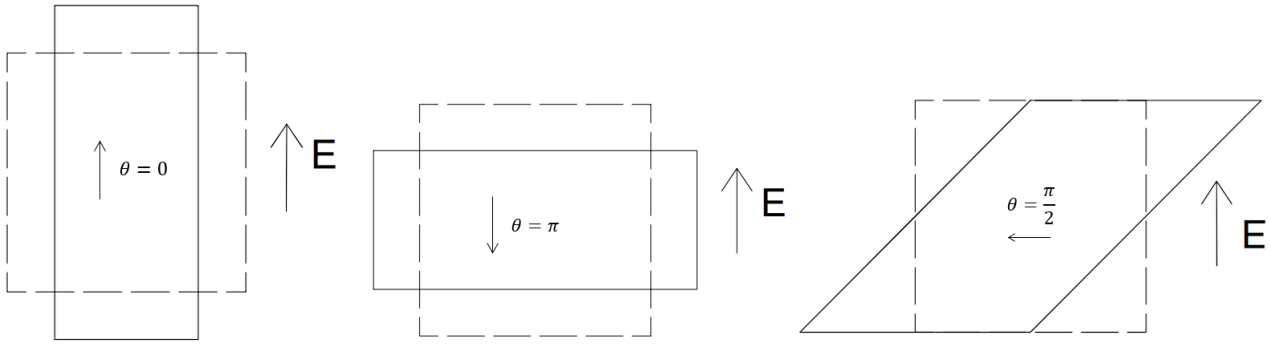

(a) (b) (c)

Figure 3.1 – Behavior of piezoelectric materials on an electric field with (a) $\theta = 0$, (b) $\theta = \pi$, and (c) $\theta = \pi/2$.

directions. A shear effect can be seen when the angle between polarization and electric field is in between the previous values.

3.2 Piezoelectric constitutive equations

The electromechanical properties presented in this work are in conformity with IEEE [Tiersten, 1967] standards. The assumption that the piezoelectric materials present a linear behavior is valid for lower levels of mechanical tension and electric fields [Gonçalves, 2019]. The constitutive equations are obtained based on the assumption that the total deformation is the sum of the deformation made by mechanical stress and by the application of an electric potential.

With $\mathcal{U}$ being the energy density, E_i the electric vector field and D_i the electric displacement vector, the electric enthalpy $\mathcal{H}$ can be defined as

$$\mathcal{H} = \mathcal{U} - E_i D_i \tag{3.1}$$

By deriving Equation 3.1 with respect to time, using the chain rule, Equation 3.2 is obtained:

$$\dot{\mathcal{H}} = \dot{\mathcal{U}} - D_i \dot{E}_i - E_i \dot{D}_i \tag{3.2}$$

The energy conservation for a linear piezoelectric material can be expressed by Equation 3.3 [IEEE, 1988].

$$\dot{\mathcal{U}} = \sigma_{ij} \dot{S}_{ij} + E_i \dot{D}_i \tag{3.3}$$

With σ_{ij} representing the mechanical stress tensor and $\dot{S}_{ij}$ the derivative over time of the deformation tensor. An equation showing that mechanical deformation and electric field are independent variables for the electric enthalpy is obtained by combining Equations 3.2 and 3.3, as

$$\dot{\mathcal{H}} = \sigma_{ij}\dot{S}_{ij} - D_i\dot{E}_i. \tag{3.4}$$

With $\mathcal{H}$ being a function of the deformation tensor and the electric vector field, $\mathcal{H}(S_{ij}, E_i)$, Equation 3.4 can be rewritten as

$$\mathcal{H} = \frac{1}{2}c^E_{ijkl}S_{ij}S_{kl} - e_{kij}E_kS_{ij} - \frac{1}{2}\varepsilon^S_{ij}E_iE_j \tag{3.5}$$

where c^E_{ijkl}, ε^S_{ij} and e_{ikl} are, in order: the elasticity tensor, with the superscript E denoting a constant electric field for the acquisition of the data; the piezoelectric tensor in the absence of mechanical strain, denoted by the superscript S; and the dielectric tensor. The elasticity tensor is a fourth-rank tensor describing the relation between stress and strain in a linear elastic material [Cowin, 1989]. The third-order linear piezoelectricity tensor relates the effect of an electric field on mechanical stress. The dielectric tensor describes the linear transformation from the external electric field to the internal electric displacement field in anisotropic materials [Liu et al., 2009]. Knowing that

$$\begin{aligned} \tfrac{\partial\mathcal{H}}{\partial S_{ij}} &= \sigma_{ij} \\ \tfrac{\partial\mathcal{H}}{\partial E_i} &= -D_i \end{aligned} \tag{3.6}$$

and partially derivating the enthalpy (Equation 3.5) with respect to its variables results in

$$\begin{aligned} \sigma_{ij} &= c^E_{ijkl}S_{kl} - e_{kij}E_k \\ D_i &= e_{ikl}S_{kl} + \varepsilon^S_{ij}E_j. \end{aligned} \tag{3.7}$$

These equations are the base for the FEM model definition. They can be further simplified by the use of Voigt's notation. By utilizing the inherent symmetries on the mechanical tensors, the sub-indices can be grouped in pairs, reducing the dimensions of the tensors. With *i, j, k, l* representing the Cartesian space, with sub-indices of 1,2 and 3, corresponding to *x, y*, and *z*, Voigt's notation groups the indices in pairs, resulting in, at most, two new sub-indices: *p* and *q*. The rules for these new indices are[Montagner,

2008]:

$$\begin{cases} p = i & if \quad i = j \\ p = 9 - i - j & if \quad i \neq j \end{cases} \tag{3.8}$$

Utilizing this notation, p and q can have values from 1 to 6, representing all possible combinations of x, y, and z. The set of constitutive equations for a piezoelectric material using Voigt's notation, reads as

$$\begin{aligned} \sigma_p &= c_{pq}^E S_q - e_{kp} E_k \\ D_i &= e_{iq} S_q + \varepsilon_{ij}^S E_j \end{aligned} \tag{3.9}$$

with the plane stress assumption defining the optimization problems described in this dissertation, the matrices can be further simplified.

3.2.1 Plane Stress and rotation

A problem with a state of plane stress has the axis perpendicular to the studied plane assumed to have negligible stress. With the plane being x-y (1-2), the stresses σ_3, σ_4, and σ_5 are all defined as zero. This is the common Kirchhoff assumption in a simple plate and shell theory. Before applying this condition to the constitutive equations, an extra step is needed. The optimization problems in this dissertation have the polarization angle of the piezoelectric material be in the plane 1-2, therefore, the constitutive values of the material need to be corrected, since the values presented in most of the literature for a piezoceramic have the polarization of the material in the z-axis.

To have the polarization of the piezoelectric material be in the xy plane, the tensors are required to rotate. The rotation to align the former z-axis with the plane is done with rotation matrices. ψ is the angle of the rotation, assuming a rotation along the x-axis, 90^{o} degrees counter-clockwise, the new y coordinate aligns with the original z, making the polarization be in the plane. The rotation of the elasticity tensor can be implemented using Equation 3.10,

$$\breve{c}^E = \boldsymbol{K} c^E \boldsymbol{K}^T \tag{3.10}$$

with

$$\boldsymbol{K}_x^{[6]}(\psi) = \begin{bmatrix} 1 & 0 & 0 & 0 & 0 & 0 \\ 0 & (\cos\psi)^2 & (\,\mathrm{sen}\,\psi)^2 & 2\cos\psi\,\mathrm{sen}\,\psi & 0 & 0 \\ 0 & (\,\mathrm{sen}\,\psi)^2 & (\cos\psi)^2 & -2\cos\psi\,\mathrm{sen}\,\psi & 0 & 0 \\ 0 & -\cos\psi\,\mathrm{sen}\,\psi & \cos\psi\,\mathrm{sen}\,\psi & (\cos\psi)^2 - (\,\mathrm{sen}\,\psi)^2 & 0 & 0 \\ 0 & 0 & 0 & 0 & \cos\psi & -\,\mathrm{sen}\,\psi \\ 0 & 0 & 0 & 0 & \mathrm{sen}\,\psi & \cos\psi \end{bmatrix}$$

$$\boldsymbol{K}_x^{[3]}(\psi) = \begin{bmatrix} 1 & 0 & 0 \\ 0 & \cos\psi & -\,\mathrm{sen}\,\psi \\ 0 & \mathrm{sen}\,\psi & \cos\psi \end{bmatrix}$$

the same is true for e and ε^S, using the equations presented in the second column of table 3.1.

The matrix $\boldsymbol{K}$ is the rotation matrix for a tensor of dimensions determined by the number in brackets on the superscript along the axis denoted by the subscript. The superscript T represents the transpose of a matrix and the angle in parenthesis represents the angle of rotation, counter-clockwise. The rotation matrices presented above are for a rotation in the x-axis and $\breve{c}^E$ is the new coordinate system of the tensor.

Applying the plane stress condition after the rotation, the remaining strains S_3, S_4, S_5 are not necessarily zero but may be calculated after the primary system is solved. The $\acute{c}^E$ constants do not have a one-to-one correspondence to $\breve{c}^E$, the simplified version of the constants derived from a fully three-dimensional analysis [Junior et al., 2009]. The relationship between the full three-dimensional constants to the plane stress is given below, the same is true for the piezoelectric and dielectric constants.

$$\begin{array}{lll} \acute{c}^E_{11} = \breve{c}^E_{11} - \frac{(\breve{c}^E_{13})^2}{\breve{c}^E_{33}} & \acute{c}^E_{22} = \breve{c}^E_{22} - \frac{(\breve{c}^E_{23})^2}{\breve{c}^E_{33}} & \acute{c}^E_{66} = \breve{c}^E_{66} \\ \acute{c}^E_{12} = \breve{c}^E_{12} - \frac{\breve{c}^E_{13}\breve{c}^E_{23}}{\breve{c}^E_{33}} & \acute{\varepsilon}^S_{33} = \breve{\varepsilon}^S_{33} + \frac{(\breve{e}_{33})^2}{\breve{c}^E_{33}} & \\ \acute{e}_{31} = \breve{e}_{31} - \frac{\breve{c}^E_{13}\breve{e}_{33}}{\breve{c}^E_{33}} & \acute{e}_{32} = \breve{e}_{32} - \frac{\breve{c}^E_{23}\breve{e}_{33}}{\breve{c}^E_{33}} & \end{array} \tag{3.11}$$

Using these equations, the elastic tensor can be simplified to a 3x3 matrix. Analogously, the e_{iq} tensor, can be reduced from a 3x6 to a 2x3 representation, similar behavior happens with the tensor ε_{ij}, changing from a 3x3 to a 2x2 matrix. Equation 3.12 shows

the new tensors in a plane stress problem with the z-axis perpendicular to the plane.

$$\acute{c}^E_{PZT} = \begin{bmatrix} \acute{c}^E_{11} & \acute{c}^E_{12} & \acute{c}^E_{16} \\ & \acute{c}^E_{22} & \acute{c}^E_{26} \\ Sym. & & \acute{c}^E_{66} \end{bmatrix}, \; \acute{e}_{PZT} = \begin{bmatrix} \acute{e}_{11} & \acute{e}_{12} & \acute{e}_{16} \\ \acute{e}_{21} & \acute{e}_{22} & \acute{e}_{26} \end{bmatrix}, \; \acute{\varepsilon}^S_{PZT} = \begin{bmatrix} \acute{\varepsilon}^S_{11} & \acute{\varepsilon}^S_{12} \\ Sym. & \acute{\varepsilon}^S_{22} \end{bmatrix} \tag{3.12}$$

Since the piezoelectric materials are not isotropic, it is important to consider the influence of the rotation angle of the piezoelectric material along the z-axis in the values of the tensors. The constants present in Equation 3.12 have the polarization aligned with the vertical y axis. To obtain the values for any other angle, the tensors need to be recalculated. With $\boldsymbol{T}$ and $\boldsymbol{R}$ rotation tensors, expressed in Equation 3.13, the new coordinates system represented by the superscript $[\grave{(\cdot)}]$, can be calculated [Carbonari et al., 2007]. Table 3.1 presents a summary of the steps toward the matrices that can be used in the problem. First, the rotation in the x-axis to align the y, then the reduction, and then the rotation if needed of the polarity.

$$\boldsymbol{T} = \begin{bmatrix} \cos^2\theta & \text{sen}^2\theta & \text{sen}\,\theta\cos\theta \\ \text{sen}^2\theta & \cos^2\theta & -\text{sen}\,\theta\cos\theta \\ -2\,\text{sen}\,\theta\cos\theta & 2\,\text{sen}\,\theta\cos\theta & \cos^2\theta - \text{sen}^2\theta \end{bmatrix}, \; \boldsymbol{R} = \begin{bmatrix} \cos\theta & \text{sen}\,\theta \\ -\text{sen}\,\theta & \cos\theta \end{bmatrix} \tag{3.13}$$

Tensors	First Rotation	Plane Stress	Rotation along z-axis
c^E	$\breve{c}^E = \boldsymbol{K}^{[6]}_x c^E \boldsymbol{K}^{[6]T}_x$	$\breve{c}^E \rightarrow \acute{c}^E$	$\grave{c}^E = \boldsymbol{T}^T \acute{c}^E \boldsymbol{T}$
e	$\breve{e} = \boldsymbol{K}^{[3]}_x e \boldsymbol{K}^{[6]}_x$	$\breve{e} \rightarrow \acute{e}$	$\grave{e} = \boldsymbol{R}^T \acute{e} \boldsymbol{T}$
ε^S	$\breve{\varepsilon}^S = \boldsymbol{K}^{[3]}_x \varepsilon^S \boldsymbol{K}^{[3]}_x$	$\breve{\varepsilon}^S \rightarrow \acute{\varepsilon}^S$	$\grave{\varepsilon}^S = \boldsymbol{R}^T \acute{\varepsilon}^S \boldsymbol{R}$

Table 3.1 – Rotation of tensors.

3.3 Compliant mechanisms

A mechanical device capable of transferring or transforming motion, energy, or force is called a mechanism. In traditional rigid-body mechanisms, the energy is conserved between input and output, disregarding friction losses. A compliant mechanism also transfers or transforms motion, energy, or force, but unlike the rigid body mechanism, CMs gain some or all of their mobility from the deflection of flexible members rather than movable joints only [Howell, 2001]. By deforming the mechanism, part of the input energy

is stored in the form of strain energy, if the device was rigid the mechanism would be a structure instead.

The advantages of using a compliant mechanism instead of a rigid body one can be separated into two categories: cost reduction and performance gain. CMs have a potential for reduction in the total number of parts, having fewer (or none) movable joints, the assembly time for these mechanisms are drastically lower than their counterpart. Compliant mechanisms can also have a simplified manufacturing process, needing fewer processes, reducing the overall cost [Howell, 2001]. Fewer movable joints result in reduced wear and decrease the need for lubrication, a desirable characteristic for difficult-to-access mechanisms or for operation in harsh environments. Another benefit of low joint count is the increase in the mechanism precision: fewer gaps and less or no backlash makes the compliant mechanism a design option for high-precision instrumentation.

The energy stored in the form of strain energy is similar to the energy stored in a deflected spring, and this similarity can be used in the design of a compliant mechanism. This characteristic can also be used to design specific properties, for instance, constant output force regardless of input displacement. In Figure 3.2a a regular clothespin is presented. In Figure 3.2b the same object is disassembled to show its three components; a spring and two rigid bodies. The clothespin uses the deformation of the spring to store energy and ensure grip strength between the rigid parts. A compliant counterpart, shown in Figure 3.2c, is made of a single piece, requiring no assembly and performing the same function. Another advantage of CMs is their scalability. With the reduction in the number of parts, the fabrication of micromechanisms using compliant mechanisms has taken off in the form of MEMS.

Compliant mechanisms are not without challenges and disadvantages. The energy-storing capacity can be used as a tool, but also means that the mechanism always retains some of the energy input, hindering the efficiency of a mechanism. Fatigue can be detrimental in the life cycle of a compliant mechanism and needs to be accounted for in cyclic uses. Other minor issues involve stress relaxation or creep, the inability to produce a continuous circular motion, and the strength limitation created by the strength of the deflecting members. In this work a time-independent solution will be created, meaning no creep of fatigue will be taken into consideration.

The desirable behavior of a CM has conflicting requisites, the mechanism needs to

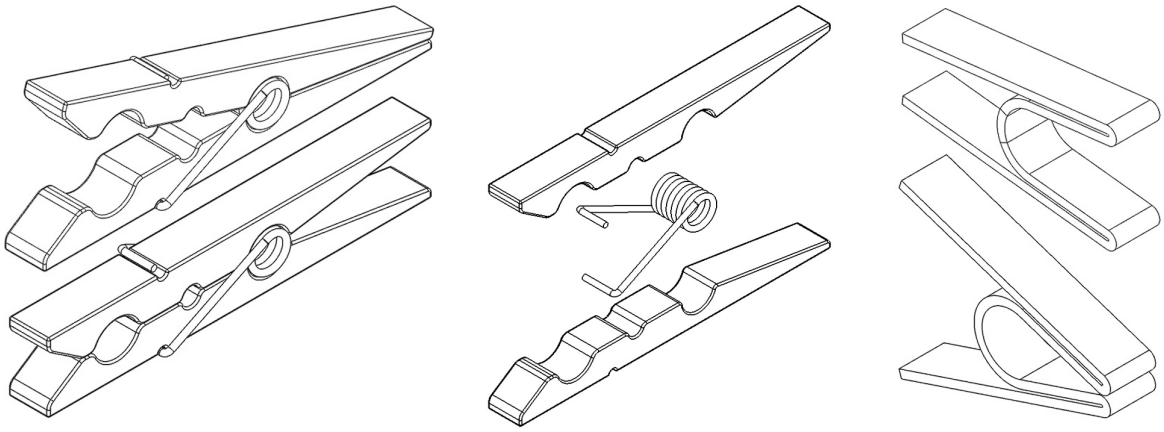

(a) (b) (c)

Figure 3.2 – (a) A spring-loaded mechanism, (b) its components, and (c) a compliant mechanism equivalent.

be rigid enough to transmit energy and be flexible enough to bend and operate [Sigmund, 1997]. Some of the possible ways to evaluate the performance of compliant mechanisms are: the geometry advantage proportionated by the mechanism, a ratio between the input and the output displacement; mechanical advantage, a comparison between the input force and the obtained by the mechanism as output; and energy conversion efficiency, a measurement of how much energy is transmitted in the device [Abdalla et al., 2005]. Another problem in dealing with CMs is the difficulty in analyzing and designing the device, especially for distributed compliance, different approaches are studied in this field, to mitigate this problem [Bahia, 2005].

3.4 Topology optimization

In mathematics, an optimization problem is defined as the problem of finding the best solution from a set of all possible solutions. In the study of structures, the optimization can be separated into three: Sizing optimization, when the only parameters changing are Cartesian scaling; Shape optimization, when the outer boundary of the structure is modified to solve the problem; and topology optimization, when the aim is to optimize material layout within a given design space.

Topology optimization usually has, as input variables, applied loads, possible support conditions, volume constraints of the structure to be manufactured, and possibly

some additional design restrictions such as the location and size of prescribed holes or solid areas, with the goal of maximizing the performance of the system. In the most generic approach, topology optimization should consist of the determination of the existence of material in every point on the design space [Sigmund and Maute, 2013]. In a FEM discretization of the real problem, the continuous space is replaced by elements, making the topology optimization a mesh-dependent process and a discrete optimization problem.

The SIMP method works by allowing intermediate values between the Young modulus of the material and the void. To each element is prescribed a variable, usually called pseudo density, ranging from zero - representing the void- and one - representing material- and the set of values for the entire domain is the solution to the optimization problem. The intermediate values, also called grey areas, are undesirable results, for the interpretation of these values is material that has less resistance than the one being optimized and more than the void, meaning a mixture of both. To skew the results from values in between the limits of the variable, a penalization is applied, making values closer to zero or closer to one. The SIMP method proposes a polynomial interpolation function to characterize the material properties of the intermediate values, the Equation 3.14 shows the classic interpretation of the method [Andreassen et al., 2010].

$$Y = Y_{min} + (Y_0 - Y_{min})(\rho^{\eta}) \tag{3.14}$$

with Y being the Young's Modulus for each element of the FEM mesh, Y_{min} a positive small value to represent the void mechanical characteristic and avoid singularities on the stiffness matrix and consequently a ill-conditioned problem, Y_0 the elastic modulus of the isotropic material chosen, ρ the variable pseudo density and η the penalization defined by the user. The most usual value for the penalization is 3, a smaller value has little impact on ρ, and a higher value can lead to nonconvergence of solutions. In Figure 3.3 a graph of the relative elastic modulus for different values of penalty factors is presented. With an increase of exponential value for the pseudo density, all in-between values of ρ are penalized towards the void characteristics, making the existence of grey areas more ineffective in the optimization problem.

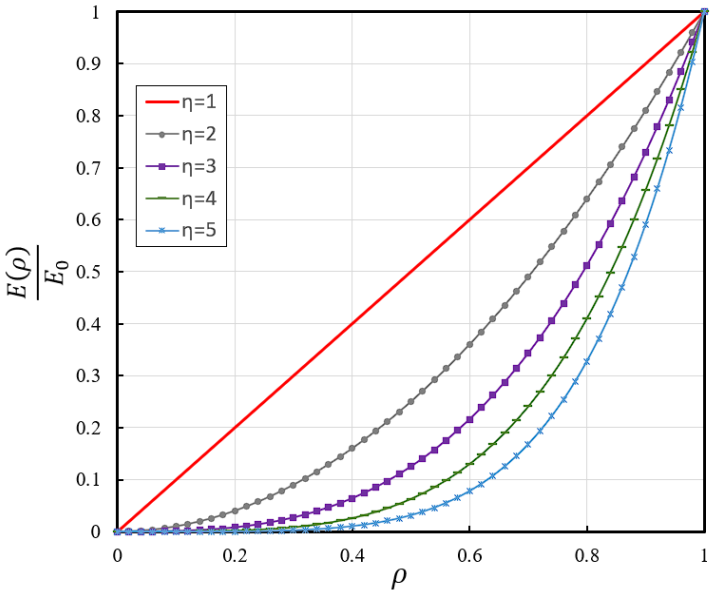

Figure 3.3 – Penalization of the intermediate densities in the SIMP model.

The SIMP method, as originally stated, can solve problems with two phases, material, and void, or, if Y_{min} were to be changed into a different isotropic material, between two materials. Optimization of two materials without void would not be classified as a topology problem, since the entire region would have the same topology before and after the optimization. To encapsulate another material on a TO problem, adding another phase, there are two main approaches: with multiple variables or with a single one.

The peak function interpolation technique for SIMP uses only one variable for pseudo density and instead of being penalized to approach 0 or 1, it has mid values for each other material. Although it can be faster solving and is independent of the number of materials, this approach tends to have more grey areas, requiring more upfront in terms of implementation and more post-processing to have steeper solutions [Zuo and Saitou, 2016].

The method proposed by Sigmund and Torquato [1999] has $(m-1)$ variables for a problem with m phases. In this approach the first pseudo-density defines the existence of material or void while the second variable determines if it is a certain material or not, this process continues until all the variables are calculated. For small quantities of phases, this approach is fairly easy to implement and understand, separating the optimization problem into $m-1$ sequential ones. In the problem studied, the solution requires three phases (two materials, and the void), therefore two variables were used. Equation 3.15

shows how to calculate Young's modulus using this method [Ge and Kou, 2021].

$$Y(\chi,\rho) = \chi^{\eta_a}(\rho^{\eta_b}Y_b + (1-\rho^{\eta_b})Y_a) + (1-\chi^{\eta_a})Y_{min} \tag{3.15}$$

with Y_a and Y_b being the Young's modulus for material a and b. The design variables are χ and ρ, being χ the variable that determines if the element is void or material, and ρ what material it is. The penalization η can be independent for each pseudo-density.

This method, however, cannot be directly applied to piezoelectric materials, as by definition they are not isotropic and the multi-physics of the problem means that not only the elastic behavior of the device should be optimized. The penalization can be applied to the stiffness matrix instead of Young's modulus for the mechanical equivalent of the SIMP method. This corrects the problem with anisotropy, but not with the multi-physics challenge of a piezoelectric solution. To have a counterpart for the SIMP method, Silva, together with Kikuchi and Nishiwaki [1999] developed the PiezoElectric MAterial with Penalization method. PEMAP is the extension of SIMP for piezoelectric materials, penalizing the stiffness, piezoelectric coupling, and dielectric matrices. Using the PEMAP idea and the dual material approach of Equation 3.15, the group of equations for the PEMAP method for two variables is represented by

$$\begin{aligned} c_{pq} &= \chi_n^{\eta_0}[\rho_n^{\eta_1}c_{pq}^{PZT} + (1-\rho_n^{\eta_1})c_{pq}^{ISO}] + (1-\chi_n^{\eta_0})c_{min} \\ \varepsilon_{iq} &= \chi_n^{\eta_0}\rho_n^{\eta_2}\varepsilon_{iq}^{PZT} + (1-\chi_n^{\eta_0})\varepsilon_{min} \\ e_{ik} &= \chi_n^{\eta_0}\rho_n^{\eta_2}e_{ik}^{PZT} + (1-\chi_n^{\eta_0})e_{min} \end{aligned} \tag{3.16}$$

where the superscript ISO represents an isotropic material, PZT is a piezoelectric one, and the subscript min represents a small value similar to the SIMP proposition. On the original paper, Silva and Kikuchi [1999] instead of using small values to represent the void as in Equation 3.16, utilized a restriction on the variable itself, making it $0 < \chi \leq 1$. Analyzing these equations it is easy to note that for values of χ close to 0 the element behaves as void and for values close to 1 the behavior of the material is defined by ρ: 0 making the behavior similar to the isotropic material and 1 to the piezoelectric one.

3.5 Filters

The SIMP method, and therefore the PEMAP, can have issues with the appearance of checkerboard areas on the optimal solution. Checkerboard patterns are alternating

solid and void elements, a product of numerical approximations introduced by the finite element method, causing the area to appear artificially strong [Díaz and Sigmund, 1995]. To prevent checkerboard, the use of higher order finite elements can be implemented. In topology design the use of higher order elements results in a substantial increase in CPU-time [Bendsøe and Sigmund, 2004]. Patching, nodal-based formulation, high-frequency filters, and perimeter constrain are other techniques to avoid the issue, but their implementation can be difficult, mesh-dependent, or not fully work [Bendsøe and Sigmund, 2004].

Mesh dependence refers to the problem of not obtaining qualitatively the same solution for different mesh-sizes or discretization [Fanni et al., 2013]. It has been shown that as the mesh density increases, the final design tends to have an increasing number of members of decreasing size [Zhou et al., 2001], showing a non-unique solution and a "convergence" to a microestructure, that can lead to impossible manufacture [Sigmund and Petersson, 1998].

To avoid this problems, a mesh-independent filter was used. The Helmholtz-type filter (HTF), proposed by Lazarov and Sigmund [2010] utilizes a Helmholtz-type partial differential equation (PDE) with homogeneous Neumann boundary conditions. By making the filtered variable the solution for Equation 3.17, with Equation 3.18 as its boundary condition, the filtered and unfiltered variables maintain the same sum, which makes possible the use of volume restrictions on pseudo-densities before or after the filtering.

$$-r^2\nabla^2\hat{\rho} + \hat{\rho} = \rho \tag{3.17}$$

$$\frac{\partial\hat{\rho}}{\partial\boldsymbol{n}} = 0 \tag{3.18}$$

On Equations 3.17 and 3.18, r represents the strength parameter, $\hat{\rho}$ the filtered variable, ρ the original variable, and $\boldsymbol{n}$ the normal vector to the boundary.

In Figure 3.4a, different solutions for the filtering of a one-dimensional signal are shown. The initial values are 0 and 1 and the mesh length is unitary. The right region shows what a 1D checkerboard pattern is: a high-frequency area. Changing the strength parameter r changes the damping effect of the filter, much like a length parameter would work on a mesh-dependent filter. The pattern shown is filtered to a non-binary variable, smoothing the form of the initial variable. Figure 3.4b shows the values presented in the graph as a image, where 0 is represented by black and 1 with a light gray. The HTF has

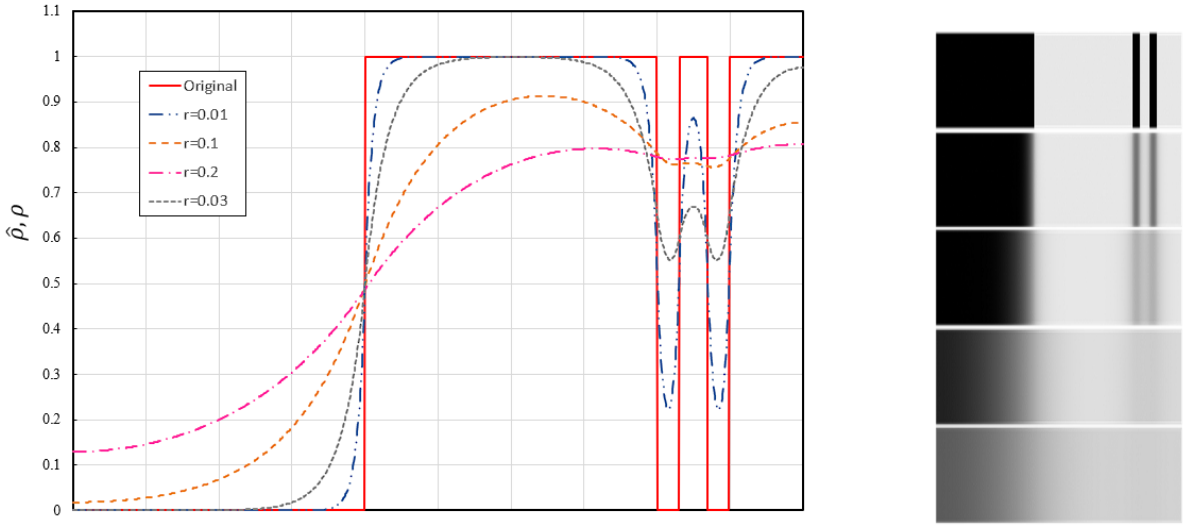

(a) (b)

Figure 3.4 – (a) Helmholtz-type filter behavior for distinct values of r. (b) A visual representation.

the tendency to depart variables from extreme values, somewhat undoing what the SIMP method tries to accomplish. To mitigate the problem, another filter can be used after it.

To further deviate the variables from mid values, some techniques can be applied. A simple threshold can be established using a Heaviside function, where any value below it is reduced to 0 and any above increases to 1. The problem with this approach is the non-continuous nature of the step function, its non-differentiability hindering the ability to calculate gradients. Sharpening the values using methods similar to image processing ones can be an alternative, but they are mesh dependent. The smooth Heaviside function (SHF) is a continuous take on the step function and was chosen to project the values towards the extremes in this dissertation. The Equation 3.19 presents the filter [Leon et al., 2015].

$$\tilde{\rho}_i = \frac{\tanh(\beta\alpha) + \tanh\left(\beta(\hat{\rho}_i - \alpha)\right)}{\tanh(\beta\alpha) + \tanh(\beta(1-\alpha))} \tag{3.19}$$

With $\tilde{\rho}_i$ being the projected variable $\hat{\rho}_i$, β determinating the slope of the function and α the threshold. In Figure 3.5 different values and their behavior on the function are shown, if not explicit, the α variable is set to 0.5, the mid value. The projection filtering has a simple implementation, however, it does not guarantee that the sum of the variables remains the same after projection, meaning that the use of this projection alters

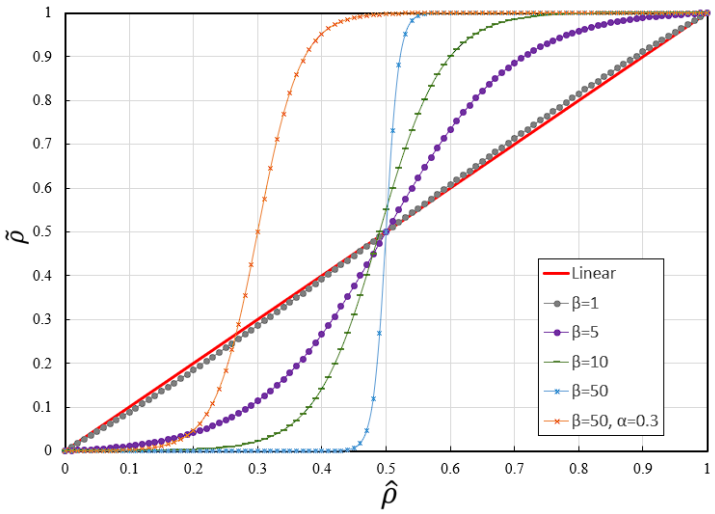

Figure 3.5 – Smooth Heaviside filter behavior.

the volume of the solution. The slope of the function can drastically change the behavior of the optimization [Leon et al., 2015], because of this, it's usual to start with a small value and increase it with each iteration.

Using both filters in the example presented in Figure 3.4a, the one-dimension checkerboard, Figure 3.6 was constructed. The first image is the original signal. The second signal shows the HTF applied, with damped values. The third and final signal is the projection of SHF used after the initial filter, creating a signal similar to the original but continuous and without the high-frequency checkerboard problem. Figure 3.6d is a visual representation of these three steps. An image post-process comparison can be made with how each filter works: HTF works similarly to a blur effect and SHF works as a sharpening in the contrast.

3.6 Solvers

Optimization problems can be solved in three major ways, analytically, graphically, and numerically. Analytical forms are divided into differential and variational calculus, both being restricted to simple optimization problems [Silva, 2007]. The graphical solutions are restricted to only two variables, leaving numerical approaches as the only viable solution for the proposed problem [Silva, 2007].

The generic numerical solutions are separated into subfields, each with a distinct ideology. Heuristics methods such as evolution programming, genetic algorithms, and

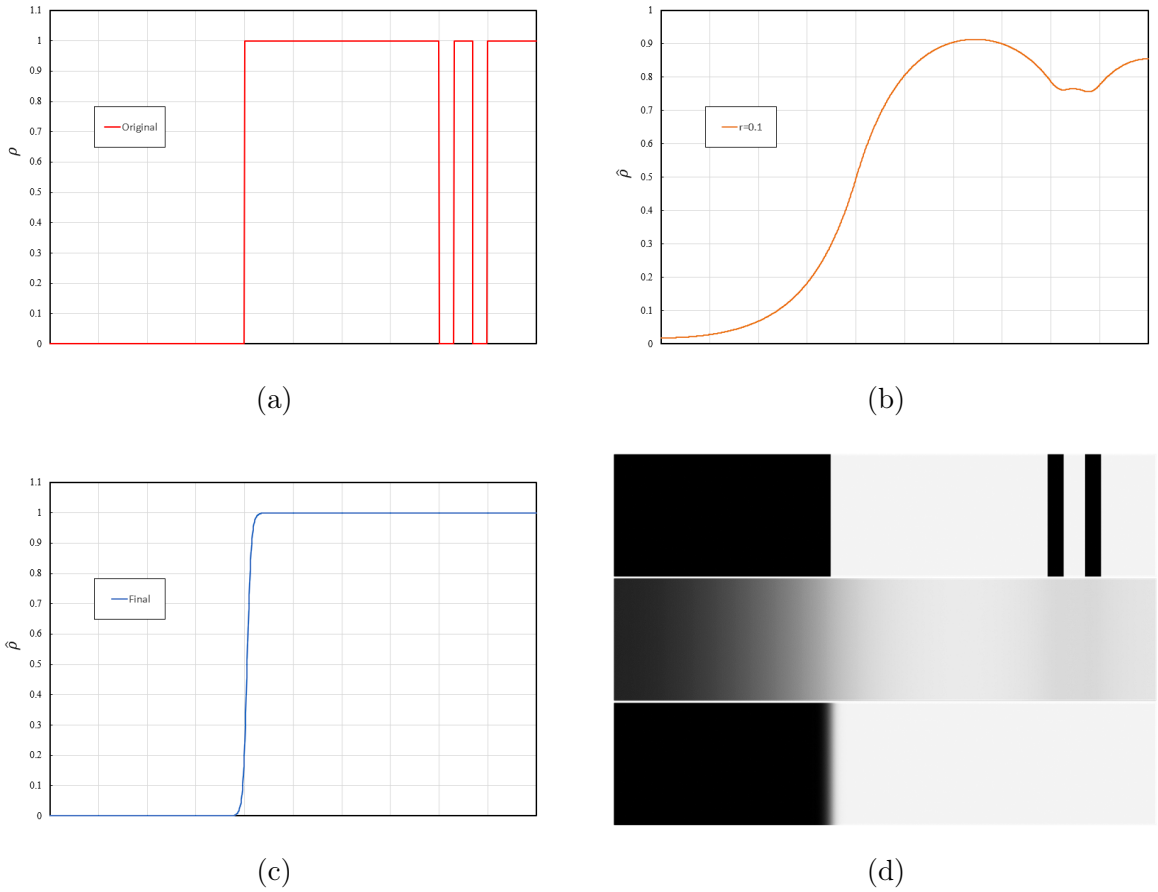

Figure 3.6 – (a) Original signal example, (b) signal after Helmholz filter, (c) final signal, after HTF and SHF. (d) A visual representation of the values shown prior.

differential evolution, have no assumptions about the problem being optimized but their computational cost increases considerably with the size of project variables [Silva, 2007]. Convex programming is a particular case of nonlinear programming, where all variables are convex functions. Convex approximation methods generate and solve a sequence of explicit approximate problems until the optimal solution of the original problem is reached [Svanberg, 1987]. Equation 3.20 shows the standard optimization problem.

$$\begin{aligned} \underset{x}{\text{minimize}} \quad & f_0(\boldsymbol{x}) \\ \text{subject to} \quad & g_i(\boldsymbol{x}) \leq 0, \quad i = 1, \ldots, m \\ & h_j(\boldsymbol{x}) = 0, \quad j = 1, \ldots, w \end{aligned} \tag{3.20}$$

with $f_0(\boldsymbol{x})$ being the objective function to be minimized, $g_i(\boldsymbol{x})$ the inequality constraint functions, $\boldsymbol{x}$ the vector of design variables and $h_j(\boldsymbol{x})$ the equality constrains. m and w

variables are the number of inequality and equality constraints, respectively. While solving the problem, inaccurate approximations can cause numerical difficulties, conservative approximations lead to slow convergence and faster approximations to oscillation. The Method of Moving Asymptotes (MMA), developed by Svanberg [1987], uses upper and lower moving asymptotes to adjust the curvature of the approximate functions. Selection of the moving asymptotes is largely heuristic [Svanberg, 1987].

The approach consists in solving the first iteration with initial guesses, calculating the objective function and its gradient; approximating a subproblem, with the functions replaced by particular convex functions, determined by the gradient and the upper and lower boundary; solving this subproblem and, with the result, creating the initial guesses for the next iteration. The code implemented in this dissertation uses a code written by Arjen Deetman Deetman over the Matlab work done by Krister Svanberg Svanberg for the application of MMA, both under the terms of GNU General Public License as published by the Free Software Foundation. It solves the following optimization problem:

$$\begin{aligned} \underset{x}{\text{minimize}} \quad & f_0(\boldsymbol{x}) + a_0 z + \sum \left(c_i y_i + \frac{d_i y_i^2}{2} \right) \\ \text{subject to} \quad & f_i(\boldsymbol{x}) - a_i z - y_i \leq 0, \quad i = 1, \ldots, m \\ & z \geq 0, \; y_i \geq 0, \qquad\quad i = 1, \ldots, m \\ & \underline{x_j} \leq x_j \leq \bar{x_j}, \qquad\quad j = 1, \ldots, n \end{aligned} \tag{3.21}$$

with f_i being the constraint functions, n being the numbers of variables, $\underline{x_j}$ and $\bar{x_j}$ representing the minimum and maximum value for each individual x_j. z and $\boldsymbol{y}$ (formed by y_i components) are auxiliary scalar and vector variables and the others (a_0, a_i, c_i and d_i) are input weights. To transform Equation 3.21 problem to one similar to that on Equation 3.20, first a_0 needs to equal one, and $a_i = 0$, then z will equal 0 in any optimal solution. Further, letting d_i be one and c_i a large number, the variable y_i becomes "expensive", pointing it to be equal to zero.

For the use of a convex approximation method, the gradient of $f_0(\boldsymbol{x})$ needs to be calculated every iteration. An efficient way of calculating this is the use of the adjoint method. The adjoint state is a numerical method for efficiently computing the gradient of a function or operator in a numerical optimization problem [Plessix, 2006]. Considering $F(\zeta, A_n) = 0$ is the forward model defined by the PDE of the governing equations, where A_n is generic project variable A_n (were A_n can represent χ or ρ) and ζ is the solution

vector. $J(\zeta, A_n)$ is the defined functional of interest. Applying the chain rule on $\frac{dJ}{dA_n}$ results in [de Miranda Kian]

$$\frac{dJ}{dA_n} = \frac{\partial J}{\partial \zeta}\frac{d\zeta}{dA_n} + \frac{\partial J}{\partial A_n} \tag{3.22}$$

and the derivative of ζ can be obtained by taking the derivative of the FEM system of equations, since the PDE operator F is defined in explicit form.

$$\frac{\partial F}{\partial \zeta}\frac{d\zeta}{dA_n} + \frac{\partial F}{\partial A_n} = 0 \tag{3.23}$$

$$\frac{d\zeta}{dA_n} = -\left(\frac{\partial F}{\partial \zeta}\right)^{-1}\frac{\partial F}{\partial A_n} \tag{3.24}$$

Applying Equation 3.24 in Equation 3.22 results in

$$\frac{dJ}{dA_n} = -\frac{\partial J}{\partial \zeta}\left(\frac{\partial F}{\partial \zeta}\right)^{-1}\frac{\partial F}{\partial A_n} + \frac{\partial J}{\partial A_n} \tag{3.25}$$

Defining the adjoint vector $(\lambda*)$ as

$$\lambda* = -\left(\frac{\partial F}{\partial \zeta}\right)^{-1} \tag{3.26}$$

with $*$ representing the complex conjugate of the transpose.

The adjoint method first solves the adjoint equation $\frac{\partial F*}{\partial \zeta}\lambda = \frac{\partial J*}{\partial \zeta}$ and them uses the adjoint solution to compute the functional gradient $\frac{dJ}{dA_n} = \lambda * \frac{\partial F}{\partial A_n} + \frac{\partial J}{\partial A_n}$.

After an optimized topology is calculated, the discreteness of this topology can be measured by a gray-level indicator as introduced by Sigmund [2007]. Equation 3.27 shows how to calculate the discreteness. M_{nd} being the measure of non-discreteness with $0(\%)$ meaning a converged design is fully discrete, that is, there are no elements with intermediate density values. For a design totally grey, all elements' densities are equal to 0.5, and M_{nd} is $100(\%)$. The $\tilde{\rho}_i$ represents the variable and n the number of variables that make the problem.

$$M_{nd} = \sum_{i=1}^{n}\frac{4\tilde{\rho}_i(1-\tilde{\rho}_i)}{n} \tag{3.27}$$

4 METHODOLOGY

In this chapter, the workflow for optimizing the topology of a compliant mechanism with piezoelectric material is shown. The methodology here presented was developed for a two-dimension problem but can be applied to a three-dimensional one. The first section presents the finite element method used. The definition of the optimal problem is, then, explained, followed up by the objective function definition. The sensitivity analysis and the method of moving asymptodes are then explored. Finalizing the chapter, the post processes and the code structure are explained.

4.1 FEM formulation

The finite element method (FEM), a general numerical method for solving partial differential equations, requires a particular space discretization in the space dimensions, which is implemented by the construction of a mesh: a numerical domain with a finite number of points. A boundary value problem is a differential equation subjected to boundary conditions. Boundary conditions specify the values that a function (Dirichlet), or the derivative of a function (Neumann), needs to take along the contour of the domain. Most applications have displacement restrictions on parts of the boundary, those, along with electric potential, can be described with Dirichlet's (first-type) boundary conditions.

To solve a boundary value problem using the FEM, two steps are required: In the first step, the original problem is rephrased in its weak form. The second step is discretization, where the weak form is discretized in a finite-dimensional space. The weak form of a piezoelectric problem, stated by Carbonari et al. [2007], is written as

$$\int_\Omega \boldsymbol{\sigma} : \boldsymbol{S} d\Omega + \int_\Omega \boldsymbol{D} \cdot \boldsymbol{E} d\Omega = \int_\Omega \boldsymbol{b} \cdot \boldsymbol{u} d\Omega + \int_\Gamma \boldsymbol{t} \cdot \boldsymbol{u} d\Gamma + \int_\Gamma Q \cdot \phi d\Gamma. \tag{4.1}$$

Assuming no body forces ($\boldsymbol{b}$) and no electric charges (Q), the Equation 4.1 can be simplified as

$$\int_\Omega \boldsymbol{\sigma} : \boldsymbol{S} d\Omega + \int_\Omega \boldsymbol{D} \cdot \boldsymbol{E} d\Omega = \int_\Gamma \boldsymbol{t} \cdot \boldsymbol{u} d\Gamma. \tag{4.2}$$

The solution for Equation 4.2 is a set of values for each finite element, $(\boldsymbol{u}, \boldsymbol{\phi})$, with $\boldsymbol{u}$ being the displacement vector and $\boldsymbol{\phi}$ the scalar value for electric potential. To obtain this result, a mixed space is required, with a vector-valued and a scalar-valued finite element functions of the Lagrangian family, with $\hat{\mathcal{V}}$ the test space and $\mathcal{V}$ the trial space. The

trial function is split into U and φ and the test function into u_{test} and v_{test}. Utilizing the definition on Equation 3.9, the Equation 4.2 can be stated as:

$$\int_{\Omega} \left(c^E \boldsymbol{S}(U) - e^T \boldsymbol{E}(\varphi)\right) : \boldsymbol{S}(u_{test}) d\Omega + \int_{\Omega} \left(e\boldsymbol{S}(U) + \varepsilon^S \boldsymbol{E}(\varphi)\right) \cdot \boldsymbol{E}(v_{test}) d\Omega = \int_{\Gamma} \boldsymbol{t} \cdot \boldsymbol{u} d\Gamma \tag{4.3}$$

$$\mathcal{V} = \{(U, \varphi) \in H^1(\Omega) : (U, \varphi) = (u, \phi) \; on \; \Gamma\}$$
$$\hat{\mathcal{V}} = \{(u_{test}, v_{test}) \in H^1(\Omega) : (u_{test}, v_{test}) = 0 \; on \; \Gamma\}$$

where $H^1(\Omega)$ is the Sobolev space. Using the definitions of symmetric strain tensor and electric field present in Equation 4.4, together with the Equations 3.16 and the appropriate boundary conditions, the FEM problem can be solved.

$$\begin{aligned} \boldsymbol{S}(\boldsymbol{u}) &= \tfrac{1}{2}\left(\nabla \boldsymbol{u} + (\nabla \boldsymbol{u})^T\right) = \boldsymbol{B}\boldsymbol{u} \\ \boldsymbol{E}(\phi) &= -\nabla \phi \end{aligned} \tag{4.4}$$

with $\boldsymbol{B}$ being the derivation operator for a 3D problem and $\acute{\boldsymbol{B}}$ the plane stress counterpart[Gonçalves, 2019].

$$\boldsymbol{B} = \begin{bmatrix} \frac{\partial}{\partial x} & 0 & 0 \\ 0 & \frac{\partial}{\partial y} & 0 \\ 0 & 0 & \frac{\partial}{\partial z} \\ 0 & \frac{\partial}{\partial z} & \frac{\partial}{\partial y} \\ \frac{\partial}{\partial z} & 0 & \frac{\partial}{\partial x} \\ \frac{\partial}{\partial y} & \frac{\partial}{\partial x} & 0 \end{bmatrix}, \acute{\boldsymbol{B}} = \begin{bmatrix} \frac{\partial}{\partial x} & 0 \\ 0 & \frac{\partial}{\partial y} \\ \frac{\partial}{\partial y} & \frac{\partial}{\partial x} \end{bmatrix}$$

The second step to solve a boundary value problem is discretization. The Python library, FEniCS project, starting from the weak form, discretizes the space according to the chosen element and directly provides, the already discretized, linear system. Equation 4.5 is the finite element equation for modeling a linear piezoelectric medium considering a static analysis, as stated by Lerch [1990].

$$\begin{bmatrix} \boldsymbol{K_{uu}} & \boldsymbol{K_{u\phi}} \\ \boldsymbol{K_{u\phi}^T} & -\boldsymbol{K_{\phi\phi}} \end{bmatrix} \begin{Bmatrix} \boldsymbol{U} \\ \boldsymbol{\phi} \end{Bmatrix} = \begin{Bmatrix} \boldsymbol{F} \\ \boldsymbol{Q} \end{Bmatrix} \tag{4.5}$$

Where $\boldsymbol{U}$, $\boldsymbol{\phi}$, $\boldsymbol{F}$ and $\boldsymbol{Q}$ are the nodal displacement, nodal electric potential, nodal mechanical force, and nodal electrical charge vectors, respectively. $\boldsymbol{K_{uu}}$, $\boldsymbol{K_{u\phi}}$ and $\boldsymbol{K_{\phi\phi}}$ are

the stiffness, piezoelectric and dielectric matrices, defined as [Piefort, 2001]

$$\boldsymbol{K_{uu}} = \int_\Omega \boldsymbol{B_u}^T c^E \boldsymbol{B_u} d\Omega$$
$$\boldsymbol{K_{u\phi}} = \int_\Omega \boldsymbol{B_u}^T e^T \boldsymbol{B_\phi} d\Omega$$
$$\boldsymbol{K_{\phi\phi}} = -\int_\Omega \boldsymbol{B_\phi}^T \varepsilon \boldsymbol{B_\phi} d\Omega$$

with $\boldsymbol{B_u} = \boldsymbol{B}\boldsymbol{N_u}$ and $\boldsymbol{B_\phi} = \nabla \boldsymbol{N_\phi}$ being the matrices derived from the interpolation functions $\boldsymbol{N_u}$ and $\boldsymbol{N_\phi}$.

4.2 Definition of the optimization problem

After the FEM formulation completed, the process of topology optimization requires the definition of the design space. With the space set, the boundary conditions can be determined, together with any external loads. The materials for the compliant mechanism need also to be determined and the desired output definition set. In a CM, the usual objective is maximizing the displacement of an output region. If the objective function was simply stated as such, the optimization would not ensure material on the region, for void is viewed as the "material" with more compliance, making the region of output a no material region, rendering an undesirable mechanism. The necessary correction on the objective function is further explained in the next section.

The design space can be one-, two-, or three-dimensional. Numerically, the space can have any natural number of dimensions other than null, but with few or no applications in engineering. Choosing a 2D plane as the domain can lead to simplification in the overall calculations by reducing a dimension. To work with a planar design space the plane stress hypothesis was used, as stated in section 3.2.

The interface between materials is assumed to be a perfect bond. No hyperelasticity was studied and the problem is considered a steady state system. The choice of materials is straightforward, with the caveat that one of the materials should be piezoelectric and the other is not required.

4.3 Objective function

In topology optimization of compliant mechanisms using piezoelectric actuators the objective of the optimization is to maximize the displacement generated in a determined region when the electric potential is applied [Silva et al., 1999b]. As previously mentioned,

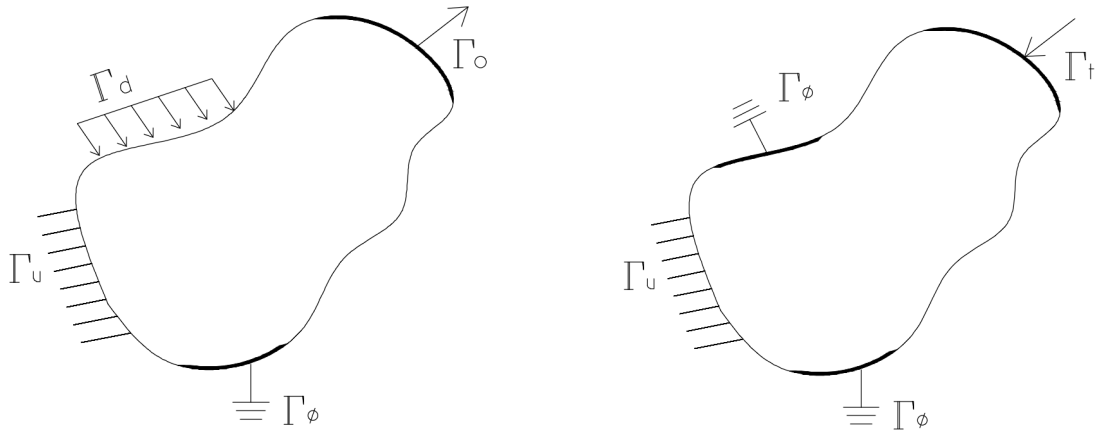

Figure 4.1 – (a) Generic piezoelectric problem and (b) the auxiliary problem

the approach to such a problem requires assurance of material in the region. For this, the problem is split into two distinct problems: the maximization of mean transduction and the minimization of mean compliance. Figure 4.1a shows the original problem where the mean transduction is calculated and the changes required in the boundary conditions to solve for the mean compliance are present in Figure 4.1b. Γ represents a boundary region, with the subscript determining its function: O represents the desirable displacement; t the mechanical dummy loads; u the prescribed displacements; ϕ represents the grounded region; and d the positive electric potential region.

The concept for mean transduction, firstly described by Silva [Silva et al., 1999a], comes from an extension of the reciprocal theorem from elasticity theory. By maximizing the mean transduction, the displacement generated by the piezoelectric is also maximized. However, if only the maximization of the mean transduction is considered, an "empty" structure can be obtained as optimal solution [Silva et al., 2003], that is, a structure with no stiffness. To solve this problem a second optimization needs to take place. By minimizing the compliance, using a dummy load in the opposite direction as the mechanism desired output, the mechanism is forced into having a connection between the output region and the rest of the CM, creating a rigid region.

Figure 4.1a represents the problem this methodology is trying to solve, a generic problem with no external forces or charges and a prescribed electric potential and displacements. Equations 4.6 and 4.7 define the mean transduction and the mean compliance,

respectively.

$$L_2(\boldsymbol{u}_1, \phi_1) = \int_{\Gamma_{\boldsymbol{t}_2}} \boldsymbol{t}_2 \cdot \boldsymbol{u}_1 d\Gamma_{\boldsymbol{t}_2} + \int_{\Gamma_{Q_2}} Q_2 \cdot \phi_1 d\Gamma_{Q_2} \tag{4.6}$$

The mean transduction is defined by the sum of two integrals, with $\boldsymbol{t}_2$ representing a dummy load in the same direction of the desired displacement, $\Gamma_{\boldsymbol{t}_2}$ the same as Γ_O, $\boldsymbol{u}_1$ the displacement calculated and Q_2 an electric charge not present in the problem described in this work, therefore, equaling zero.

$$L_3(\boldsymbol{u}_3, \phi_3) = \int_{\Gamma_{\boldsymbol{t}_2}} \boldsymbol{t}_3 \cdot \boldsymbol{u}_3 d\Gamma_{\boldsymbol{t}_2} \tag{4.7}$$

Mean compliance can be defined as the work done by external forces [Frecker et al., 1997]. The structural function of minimizing the mean compliance is to guarantee the compliant mechanism has material in the objective region. The mean compliance is calculated on the problem described by Figure 4.1b, with no electric charges and no prescribed electric field, the mean compliance is obtained through a fully mechanical problem, with $\boldsymbol{u}_3$ being the displacement in the Γ_O region and with an opposite direction dummy load defined as $\boldsymbol{t}_3 = -\boldsymbol{t}_2$.

Minimizing mean compliance while maximizing mean transduction can be achieved by maximizing a combination of Equations 4.6 and 4.7, such as Equation 4.8, proposed by Silva et al. [2000].

$$f_0^{max} = L_2/L_3 \tag{4.8}$$

Usually, an optimization problem is expressed in terms of minimizing a function. Since Equation 4.8 has the opposite goal, an inverse function can be stated, such as

$$f_0^{min} = L_3/L_2, \quad f_0^{min} = -L_2/L_3. \tag{4.9}$$

To solve an optimization problem using PEMAP, the design variables need a initial value. Typically, the first guess of any variable is a constant value in all of the domain, so as to not skew the results in any direction. This value can be the target volume for the final design, helping the convergence. Volume is used here as a generic term, meaning actual volume, for three-dimensional cases, and area for planar ones. With V_χ and V_ρ being the maximum values for the volumes of each variable, the inequalities can be stated.

$$\begin{aligned} \textstyle\int_\Omega \chi_i d\Omega &\leq V_\chi \\ \textstyle\int_\Omega \rho_i d\Omega &\leq V_\rho \end{aligned} \tag{4.10}$$

Since V is a mesh-dependent value, with a more refined mesh, more elements and greater values are obtained. To maintain a constant value while refining the mesh it is best to work with a percentage approach. With $\mathfrak{f}_\chi$ and $\mathfrak{f}_\rho$ being the maximum percentage values of volume a variable can have in the domain, V can be defined as

$$\begin{aligned} V_\chi &= \int_\Omega \mathfrak{f}_\chi d\Omega \\ V_\rho &= \int_\Omega \mathfrak{f}_\rho d\Omega \end{aligned} \tag{4.11}$$

with the pseudo densities being an array of values from zero to one, Equations 4.10 and 4.11 can be rewritten as, mesh independent, inequalities:

$$\int_\Omega (\chi - \mathfrak{f}_\chi) d\Omega \leq 0 \tag{4.12}$$

$$\int_\Omega (\rho - \mathfrak{f}_\rho) d\Omega \leq 0 \tag{4.13}$$

With the inequalities that restrict the optimization problem defined, the optimization problem of the first varialbe, χ can be defined as

$$\begin{aligned} \underset{\boldsymbol{\chi}}{\text{minimize}} \quad & f_0(\boldsymbol{\chi}) = \frac{L_3}{L_2} \\ \text{subject to} \quad & \int_\Omega (\chi_i - \mathfrak{f}_\chi) d\Omega \leq 0, \quad i = 1, \ldots, m \\ & 0 \leq \chi_j \leq 1, \qquad\qquad j = 1, \ldots, n \end{aligned} \tag{4.14}$$

Similarly, changing the variable on Equation 4.14 to ρ will result in the optimization problem being solved secondly. Variable ρ controls what percentage of the material is piezoelectric. It is advisable to have a initial value this variable with at least a continuous path between positive and negative -or ground- electric potentials boundary conditions so that for the first iteration the piezoelectric component has an electric field to influence the objective function.

To calculate the objective function there are two finite elements problems to be solved (boundary conditions (a) and (b) from Figure 4.1). The results from them are two sets of values, $(\boldsymbol{u}_1, \boldsymbol{\phi}_1)$ and $(\boldsymbol{u}_3, \boldsymbol{\phi}_3)$. Solving Equations 4.6 and 4.7 the objective function f_0 can be calculated.

4.4 Sensitivity analysis

The sensitivity analysis of the objective function express how and how much changes in the parameters of an optimization problem modify the optimal objective function value and the point where the optimum is attained [Castillo et al., 2008]. This knowledge is required to better optimize the topology and is needed to use the MMA.

The sensitivities (derivatives) can calculated with the adjoint method using the definition present in section 3.6. Equation 4.15 shows the gradient of the function $f_0 = L_3/L_2$ in respect to a generic project variable A_n (were A_n can represent χ or ρ) [Carbonari, 2003].

$$\frac{\partial f_0}{\partial A_n} = \frac{1}{L_2}\left(\frac{\partial L_3}{\partial A_n}\right) - \frac{L_3}{(L_2)^2}\left(\frac{\partial L_2}{\partial A_n}\right) \tag{4.15}$$

with the partial derivatives of L_2 and L_3 defined as

$$\begin{aligned}\frac{\partial L_2}{\partial A_n} = &- \int_\Omega \varepsilon^S(\boldsymbol{u}_2)^T \frac{\partial c^E}{\partial A_n}(\boldsymbol{u}_1)d\Omega - \int_\Omega (\nabla\boldsymbol{\phi}_2)^T \frac{\partial e^T}{\partial A_n}\varepsilon^S(\boldsymbol{u}_1)d\Omega + \\ &- \int_\Omega \varepsilon^S(\boldsymbol{u}_2)^T \frac{\partial e}{\partial A_n}\nabla\boldsymbol{\phi}_1 d\Omega + \int_\Omega (\nabla\boldsymbol{\phi}_2)^T \frac{\partial \varepsilon^S}{\partial A_n}\nabla\boldsymbol{\phi}_1 d\Omega\end{aligned} \tag{4.16}$$

$$\begin{aligned}\frac{\partial L_3}{\partial A_n} = &- \int_\Omega \varepsilon^S(\boldsymbol{u}_3)^T \frac{\partial c^E}{\partial A_n}(\boldsymbol{u}_3)d\Omega - \int_\Omega (\nabla\boldsymbol{\phi}_3)^T \frac{\partial e^T}{\partial A_n}\varepsilon^S(\boldsymbol{u}_3)d\Omega + \\ &- \int_\Omega \varepsilon^S(\boldsymbol{u}_3)^T \frac{\partial e}{\partial A_n}\nabla\boldsymbol{\phi}_3 d\Omega + \int_\Omega (\nabla\boldsymbol{\phi}_3)^T \frac{\partial \varepsilon^S}{\partial A_n}\nabla\boldsymbol{\phi}_3 d\Omega\end{aligned} \tag{4.17}$$

These partial derivatives, together with the Jacobian $\frac{\partial f_i}{\partial x_j}$ used as input vectors for the MMA subprogram.

In the case of using the FEniCS platform with dolfin-adjoint [Alonso], it is not necessary to derive the adjoint equations by hand. The program interprets the equations defined in the FEniCS enviroment and applies a generic algorithmic differentiation model resulting in the sensitivities desired.

4.5 Definition of MMA problem

The method of moving asymptotes, an optimization method, requires the input of 18 variables, with eleven of them mentioned in Section 3.6, being them: m, n, a_0, $\boldsymbol{a}$, $\boldsymbol{c}$, $\boldsymbol{d}$, $\boldsymbol{x}$, $\underline{x}_j$, $\bar{x}_j$, f_i and f_0. Of the seven remaining, five are iteration variables: previous lower and upper asymptotes, the current iteration, and the last two iterations values

for $\boldsymbol{x}$. This values are calculated within the code provided by Deetman. The final two needed variables are a column vector with the derivatives of the objective function f_0 with respect to the variables x_j($\frac{\partial f_0}{\partial x_j}$) and the $m \times n$ matrix with the derivatives of the constraint functions f_i with respect to the variable x_j ($\frac{\partial f_i}{\partial x_j}$). Both variables are obtained through the sensitivity analysis.

The output variables of the MMA problem are the five iteration variables required as inputs for the next iteration and $\boldsymbol{y}$ and z, the vector and scalar auxiliary variables, equaling 0.

The optimization problem this work proposes to solve has two variables, χ and ρ. Therefore, the MMA is split into two distinct optimization problems, one for each variable. Their solution is calculated simultaneously, that is, within the same iteration both variables are calculated.

The first variable to be iterated is χ, the pseudo density responsible to ensure the existence or nonexistence of material. In the set of Equations 3.16 the null value for the variable results in an approximate zero amount of mechanical characteristics (non-zero for computational stability). With the restriction that $\mathfrak{f}_\chi \geq \mathfrak{f}_\rho$ the first optimization problem stated in Equation 4.14 is the first variable optimization problem.

In the inner workings of the MMA solver, the maximum change a variable can have (`move`) is usually set to 0.3 (30% of the value), bigger changes can lead to not finding the local minima and smaller ones can lead to a slow convergence. Table 4.1 presents the inner parameters of the MMA solver, with the default values used in this dissertation. `epsmin` is the convergence condition for solving the MMA sub-problem, hence, it should approximate 0 to guarantee the calculation accuracy. `raa0` is associated with the second derivative of the approximate function, the optimization could be more conservative with a greater value. `albefa` have a similarly function to `move`, working by scaling the distance between the upper and lower asymptotes. `asyinit` is a parameter applied to the calculation of the asymptotes in the first two iterations. `asyincr` is used to move the asymptotes away from the current iteration point, smaller values lead to conservativeness of the optimization. Finally, `asydecr` is used to move the asymptotes closer from the current iteration [Yu et al., 2022].

Parameter	Value
`epsmin`	10^{-7}
`raa0`	10^{-5}
`move`	0.3
`albefa`	0.1
`asyinit`	0.5
`asyincr`	1.2
`asydecr`	0.7

Table 4.1 – Material properties for the beams benchmark.

4.6 Post processing

As briefly mentioned in section 3.5, the PEMAP method can have problems with checkerboard patterns or intermediate values (grey areas). To remediate those problems two solutions were used.

To reduce the occurrence of checkerboard patterns and small floating islands of material, the HTF is used after every iteration of the design variables. The filter has only one parameter r, and its value should be decided experimentally. The smaller the value of r, minor the impact of the filter on the final result. The use of a Helmholtz-type filter implies an increase in undesirable mid-values for the variables. To steer the values to desirable ranges, the projecting filter (SHF) is used in sequence after every use of HTF.

The desirable values for the design variables χ and ρ are 0 or 1, since any intermediate value represents a mixture of materials or void. Using SHF, the intermediate values can be skewed towards one of the two meaningful values while staying continuous, a desirable characteristic to calculate the derivatives required by the optimization solver (MMA). Parameter α is set to 0.5, with any larger value tending towards 1 and any smaller to 0. Increasing β increases the function slope, however, starting the problem with a large value can lead to numerical issues [Leon et al., 2015]. The approach used in this work is a continuation method, that is, starting with a small value for β and slowly increasing its magnitude after a certain number of iterations. This method is considered slow (in convergence) and can cause slight artificial perturbations to the topology [Guest et al., 2011]. The chosen rule was: starting with $\beta = 1$ and after 50 iterations doubling it, to the maximum of 128 on the 350th iteration.

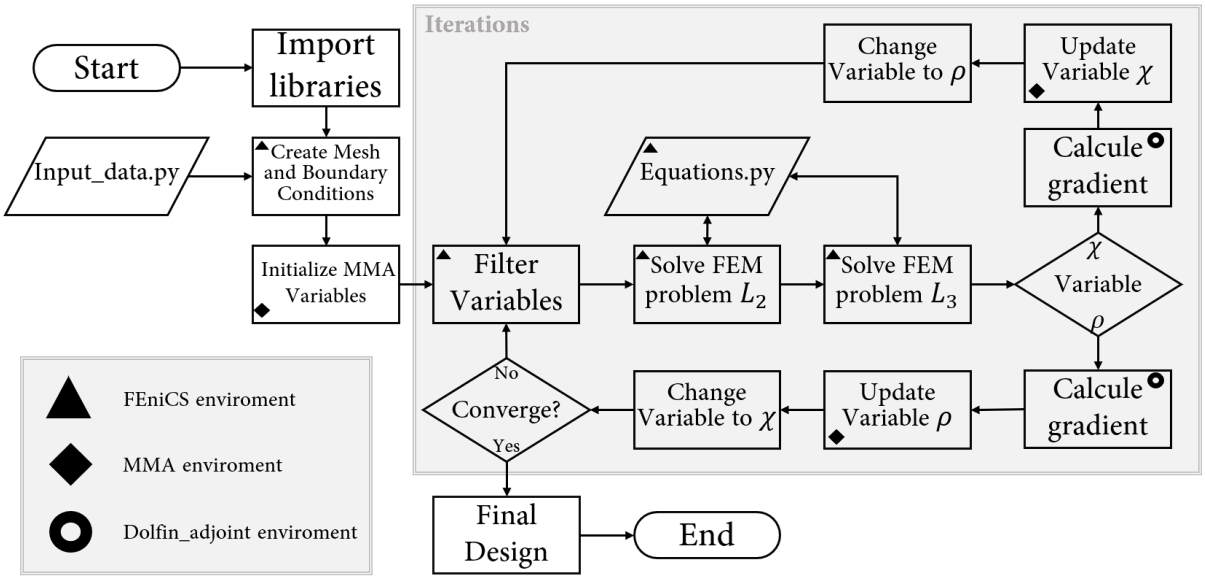

Figure 4.2 – Flowchart for the Python code

4.7 Numerical implementation

The methodology required to create a generic code that works for any 2D problem with the polarization on the plane will be expressed in this section.

The program, written in Python, requires additional libraries. Numpy is a library widely used for scientific computing, providing a multidimensional array of objects (vectors, matrices) and various mathematical operations on them [Harris et al., 2020]. UFL, or Unified Form Language, is a part of the FEniCS Project and defines a flexible interface for choosing finite element spaces and defining expressions for weak forms in a notation close to mathematical notation [Alnæs et al., 2014]. The MMA subprogram is responsible for solving the optimization problem using the method of moving asymptotes [Deetman]. The subprograms created by the author, `input_data` and `Equations` were both created to accompany the main code and have the input values and all equations described in this work. The FEniCS Project is the main library used in the program, helping the clarity and usage of it. The `dolfin_adjoint` project automatically derives the discrete adjoint and tangent linear models from a forward model written in the Python interface to FEniCS [Mitusch et al., 2019].

Figure 4.2 presents the flowchart of how the code works, with caption showing each of the main libraries used is responsible for each part.

The `main.py` python code starts by importing the libraries needed, followed by

the creation of objects with information about the problem to be solved, described in the subprogram `input_data`.

```
import numpy as np
from MMA import mmasub
from fenics import *
from dolfin_adjoint import *
from ufl import tanh
from input_data import *
from Equations import *
```

After the import of the required libraries and the creation of the mesh and subdomains such as output displacement area or the fixed support region, the boundary conditions are created (two, one for each sub-problem L_2 and L_3) as well as initializing the MMA arrays of initial variables.

```
x_1 = csi_0.vector().get_local()
x_2 = rho_0.vector().get_local()
n, m = x_1.size, 1
xmin, xmax = np.zeros((n,1)), np.ones((n,1))
xval_1, xval_2 = x_1[np.newaxis].T, x_2[np.newaxis].T
xold1_1, xold2_1 = xval_1.copy(), xval_1.copy()
xold1_2, xold2_2 = xval_2.copy(), xval_2.copy()
low_1, upp_1 = np.ones((n,1)), np.ones((n,1))
low_2, upp_2 = np.ones((n,1)), np.ones((n,1))
a0 = 1
a = np.zeros((m,1))
c = np.ones((m,1))*1e9
d = np.ones((m,1))
move, change, loop = 0.3, 1,-1
Obj_1 = np.zeros((pdat.iterations,1))
Obj_2 = np.zeros((pdat.iterations,1))
while (change > 1e-5 ) and (loop<pdat.iterations):
    loop = loop+1
    f0val_1,df0dx_1,fval_1,dfdx_1,frac_solid,frac_pzt =
```

```
Forward(x_1,x_2,1)
```

After this pre-iteration step, the filters (HTF and SHF) are applied to both variables, followed up with the calculation of both forward problems and the objective function, utilizing the `Equations` subprogram.

```
def Forward(x1,x2,switch):
csi.vector()[:], rho.vector()[:] = x1, x2
w,w2 =Function(mdat.W), Function(mdat.W)
(U, V) = TrialFunctions(mdat.W)
(utest, vtest) = TestFunctions(mdat.W)
rho_hf=helmholtz_filter(rho,fdat.r,mdat.M)
rho_pj=projecting(rho_hf,fdat,mdat.M)
csi_hf=helmholtz_filter(csi, fdat.r,mdat.M)
csi_pj=projecting(csi_hf,fdat,mdat.M)
U_form=inner(sigma_i(U,V,csi_pj,rho_pj,pdat,adat),epsilon(utest))*dx
V_form=inner(D_i(U,V,csi_pj,rho_pj,pdat,adat),-grad(vtest))*dx
F = U_form + V_form
bilinear1 = dot(Constant((0.0,0.0)),utest)*dx
bilinear2 = dot(pdat.DummyLoadNegative, utest)*dsCont(1)
problem1=LinearVariationalProblem(F,bilinear1,w,bcs=bc1)
solver1=LinearVariationalSolver(problem1)
solver1.parameters['linear_solver'] = 'umfpack'
solver1.solve()
```

Depending on what variable will be used, the sensitivity analysis are calculated by the `dolfin_adjoint`. The derivatives are calculated with respect to χ if it is the first calculation of the iteration (switch==1) or with respect to ρ if it is the second (switch==2). The last phase before the optimization solver is to change all the variables that are attributed to a mesh into a matrix or vector, making the solver strictly mathematical.

```
if switch==1:
    control = Control(csi)
    vc=UFLInequalityConstraint((csi-pdat.FracVol)*dx,control)
    fval=np.array(vc.function(csi),dtype=float)[np.newaxis]
```

```
                                                    [np.newaxis]
elif switch==2:
    control = Control(rho)
    vc=UFLInequalityConstraint((rho-pdat.FracVol_Pzt)*dx,control)
    fval=np.array(vc.function(rho),dtype=float)[np.newaxis]
                                                    [np.newaxis]
else:
    print("error")
df0dx_func = compute_gradient(f0val, control)
df0dx = df0dx_func.vector().get_local()[np.newaxis].T
dfdx = np.array(vc.jacobian(control.vector().get_local()))
```

With all the values calculated, the MMA is started and proceeds to calculate any changes in the variables. If no stop criteria is met, a new iteration occurs. After one of the stop criteria is achieved, the information is saved. Among the saved information is the history of the objective function, both variables in all iterations, as well as the output of the weak formulation, the displacement, and the electric potential. The Figure 4.2 presents a flowchart of the Python code structure.

An ill-conditioned problem is one where a small change in the input brings a large change in the output. Ill-conditioned systems are inherently difficult to solve, it can occur with matrices that have drastic changes in the order of magnitude within them. This problem can be avoided using partial pivoting, modifying the usual row reduction algorithm. UMFPACK (Unsymmetric MultiFrontal Package) is a library developed by Davis [Davis], which is designed to solve large, sparse, unsymmetric linear systems of equations. The FEniCS project utilizes of the UMFPACK solver not only in linear problems, but also within each iteration of a nonlinear solve via Newton's method, an eigenvalue solve, or time-stepping [Logg et al., 2012].

In some problems the objective function calculated can be a small value, when using the definition $f_0 = -L_2/L_3$, with an order of magnitude 10^{-7}, and with the small scale of f_0 floating errors creep up and the problem can lead to non-convergence. To solve this problem an increase in the voltage could be done, increasing the mean transduction without increasing the mean compliance or multiplying f_0 by 10^7 to bring the value to a bigger number and avoid rounding errors. Ultimately, the approach used was to solve

with $f_0 = L_3/L_2$ instead, to avoid this problem altogether.

5 RESULTS

In this chapter, the results of each step taken to develop the code for optimizing the piezoelectric material and an isotropic one in the same design domain, to create a compliant mechanism are shown. Firstly all the benchmarks are done to ensure the inner workings of each singular step and then the results for the five problems developed are discussed.

5.1 Benchmarks

To ensure the validity of the obtained results, benchmark problems were studied. Three distinct problems, each validating a different aspect of the methodology, were assessed. They are the displacement inverter mechanism, a classical compliant mechanism; an adaptive sandwich beam and a surface-mounted actuation beam for validating the multi-physics formulation; and a flextensional actuator using the methodology proposed by Silva et al. [2003], to validate the mean transduction and mean compliance approach of solving the TO problem.

5.1.1 Inverter mechanism

The inverter mechanism benchmark is a classical problem of optimization [Zheng et al., 2008]. The design domain is a square with vertical symmetry, with an input region in the middle of a side and the output in the middle of the opposing side, with two fixed corners. The objective of such mechanism is to invert the motion on the input region, that is, for a positive input displacement on the x-axis, a negative output displacement will appear. Since there is vertical symmetry, the problem can be divided by half using the correct boundary conditions, as shown in the Figure 5.1.

The methodology to solve this optimization process is similar to the methodology used for this dissertation but made simpler by virtue of the use of only one material, an isotropic one. Therefore, no multi-physics was required and, to ensure the output region had material, a dummy spring (K_{out}) was used on the boundary of the output. A input force ($\boldsymbol{t_3}$) was used as an outside force in the equilibrium equation. The created mesh for this domain, and all domains described in this dissertation, utilizes Linear Strain Triangles (LST) elements, stacked to form 2D rectangles, tiling a rectangle domain. The total

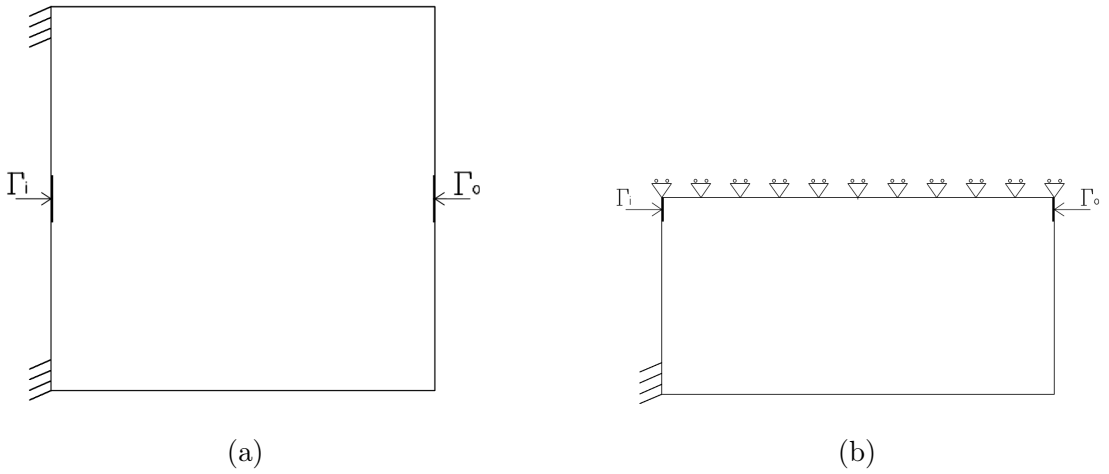

Figure 5.1 – Design domain of inverter mechanism. (a) The entire domain and (b) half domain with the boundary conditions

L[mm]	150	K_{out}	10^{-3}
$\boldsymbol{t_3}$	[1,0]	ν	0.2
Y [MPa]	1	η	3
Y_{min}	10^{-6}	r	2.1

Table 5.1 – Inverter problem specifications

number of triangles elements is $2n_xn_y$ and the total number of vertices, $(n_x+1)(n_y+1)$, n_x and n_y being the desirable number of cells in each direction, with n_x being the same as L, the size of the domain, and n_y being half of that value due to symmetry constraint, the size of each cell is equal to the unity of the problem (in this case 1 mm). The input and output regions sizes are 6.67% of the size of the side in which they appear. The table 5.1 shows the material specifications as well as the requirements of Equations 3.14 and 3.17

Figure 5.2a shows the result of the topology optimization for a maximum volume fraction of 25%. Even with a generic material and loads, the outcome represents a mechanism with similar topology and functionality of what is usual in the literature, as shown in Figure 5.2b. This benchmark validates the initial use of the FEniCS library, the MMA subprogram, and the filter used (Helmholtz-type). The mesh used for this problem consisted of 11099 triangles, the M_{nd} equal to 1.35% and, with an input displacement of 0.985 mm and an inverse displacement of 2.355 mm, the geometrical advantage [Wang, 2009]

obtained was 2.39.

(a) (b)

Figure 5.2 – (a) Final result of topology optimization and (b) an inverter obtained by Wang et al. [2017]

5.1.2 2D beams

The work of Zhang and Sun [1996] on adaptive sandwich structures and the surface-mounted counterpart allows for a comparison between the FEM, using Equation 4.3, and the governing equations based on the variational principle developed by Zhang and Sun [1996]. Figure 5.3 indicates both problems studied.

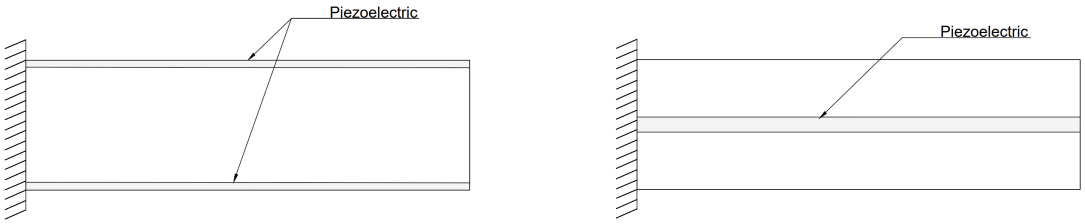

(a) (b)

Figure 5.3 – (a)Adaptive beam and (b) a surface-mounted actuation beam.

The problem described in Figure 5.3a is an adaptive beam with no external forces and a vertical current applied, the upper piezoelectric has an opposite direction of electric field and polarization while the bottom one is aligned. With the Equation 5.1, a theoretical value for the vertical displacement (w) along the length of the beam is calculated.

$$w_a = \frac{K_1 K_6}{K_2}\left(x + \frac{\sinh\left[\lambda(L-x)\right]}{\lambda\cosh\left(\lambda L\right)} - \frac{\tanh\left(\lambda L\right)}{\lambda}\right) + \frac{1}{2K_2}\left(\frac{K_1 K_5}{K_4} - 1\right)\left(\frac{1}{3}x^2 - Lx\right)x\mathfrak{D} \tag{5.1}$$

with L representing the total length of the beam, 1m, x the distance on the x-axis, $\mathfrak{D} = 0$ and λ and K_i defined as

$$K_1 = \tfrac{1}{2}\mathfrak{D}_{11} t t_c (t_c + t) + \tfrac{1}{2}\mathfrak{D}^E_{33} t_c^3$$
$$K_2 = \tfrac{1}{6}\mathfrak{D}_{11} t^2 (4t + 3t_c)$$
$$K_3 = \tfrac{1}{6}\mathfrak{D}_{11} t^2 t_c^2 + \tfrac{1}{9}\mathfrak{D}^E_{33} t t_c^3$$
$$K_4 = \tfrac{1}{3}(4t + 3t_c)\mathfrak{D}^E_{55} t_c (1 + \tfrac{K_1}{K_2})$$
$$K_5 = \tfrac{1}{3K_2}(4t + 3t_c)\mathfrak{D}^E_{55} t_c$$
$$K_6 = \tfrac{1}{3K_4}(4t + 3t_c) e_{15} E t_c + \tfrac{K_3 K_5}{K_4^2}\mathfrak{D} + \tfrac{t_c}{K_4}\mathfrak{D}$$
$$\lambda = \sqrt{\tfrac{K_4}{K_3}}$$

where t represents the top and bottom thickness, t_c the middle layer thickness, e_{15} the dielectric tensor component of the piezoelectric material, and E the electric field according to Equation 4.4. With the additional definitions of

$$\mathfrak{D}_{11} = \tfrac{Y}{(1-\nu^2)}\mathfrak{D}^E_{33} = c^E_{33} - \tfrac{(c^E_{13})^2}{c^E_{11}}\mathfrak{D}^E_{55} = c^E_{55}$$

and with c^E representing the components of the elasticity tensor of the piezoelectric material as well as Y and ν representing the elastic modulus and Poisson's coefficient of the isotropic material, respectively, the value is, compared to the displacement obtained by the FEniCS program using the multi-physics approach.

The graph presented in Figure 5.4a shows both displacements with respect to the length of the beam. The R-squared (r^2) value for the correlation between both curves is 0.999980596, a great indication of well-implemented piezoelectric FEM.

The same process happens for the surface-mounted actuation beam described by Figure 5.3b. In it, the piezoelectric layer is the middle one and the polarization in it is in the direction of the length, making it perpendicular to the applied electric field. In the original papper, Zhang and Sun study the time dependent actuation of the beam, but have the Equation 5.2 for a static solution as well.

$$w_b = \frac{-\mathfrak{D} x^3}{6EI} + \frac{1}{2EI}[\mathfrak{D} L + e^x_{31}(t + t_c) t E] x^2 \tag{5.2}$$

Equation 5.2 has e^x_{31} as one of the parameters, calculated by $e^x_{31} = e_{31} - \frac{c^E_{13} - e_{33}}{c^E_{33}}$ with EI defined as

$$EI = \frac{1}{6}\mathfrak{D}^E_{11} t^3 + \frac{1}{2}\mathfrak{D}^E_{11}(t + t_c)^2 t + \frac{1}{23}\mathfrak{D}_{11} t_c^3$$

and $\mathfrak{D}_{11}^{E} = c_{11}^{E} - \frac{(c_{13}^{E})^2}{c_{33}^{E}}$. Figure 5.4b shows a graph for the vertical displacement values, similar to the first problem. The r^2 value for the curve is 0.999902145.

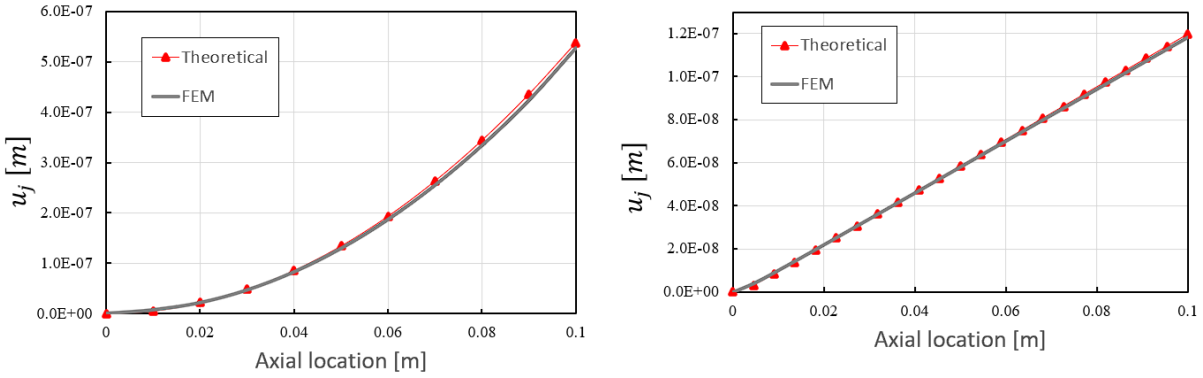

(a) (b)

Figure 5.4 – : Vertical displacement of (a) an adaptive beam and (b) a surface-mounted actuation beam

With both examples having similar results for a 2D or a 3D mesh, using the materials described in table 5.2, the benchmark was deemed correctly implemented and the FEM implementation, together with the plane stress approach, was considered accurate. The values presented in table 5.2 are the constitutive values for a PZT-5H material with polarization in the z-axis. For the surface-mounted actuation beam problem, where the polarization points towards the x-axis, a correction was used. Utilizing the equations presented in table 3.1 for the angles of $\psi = -\pi/2$ radians and $\theta = -\pi/2$ radians, the result tensors are presented in Equation 5.3.

$$
\begin{aligned}
c_{PZT}^{E} &= \begin{bmatrix} 60.867 & 31.371 & 0 \\ & 76.469 & 0 \\ Sym. & & 23 \end{bmatrix} [GPa] \\
e_{PZT} &= \begin{bmatrix} 23.3 & -6.5 & 0 \\ 0 & 0 & -17 \end{bmatrix} [\tfrac{C}{m^2}] \\
\varepsilon_{PZT}^{S} &= \begin{bmatrix} 1477.27 & 0 \\ Sym. & 1707.95 \end{bmatrix} /\varepsilon_0
\end{aligned}
\tag{5.3}
$$

PZT-5H material properties			
Elastic constants	c_{11}^E, c_{22}^E, c_{33}^E	126	GPa
	c_{12}^E	79.5	
	c_{13}^E, c_{23}^E	84.1	
	c_{44}^E	23.3	
	c_{55}^E, c_{66}^E	23	
Piezoelectric constants	e_{31}, e_{32}	-6.5	$\frac{C}{m^2}$
	e_{33}	23.3	
	e_{24}, e_{15}	17	
Dielectric constants	$\varepsilon_{11}^S/\varepsilon_0$, $\varepsilon_{22}^S/\varepsilon_0$	1707.95	–
	$\varepsilon_{33}^S/\varepsilon_0$	1477.27	
Aluminum material properties			
Elastic constants	Y	70.3	GPa
	ν	0.345	–

Table 5.2 – Material properties for the beams benchmark.

5.1.3 Flextensional actuator

The topology optimization of a flextensional actuator, described by Silva et al. [2003], uses the mean compliance and mean transduction approach to solving the optimization of a piezoelectric activated actuator. The actuator, named f2b0830, has the design constraint described in the Figure 5.5. Having a fixed piezoelectric domain and optimizing only the nonpiezoelectric material, a static solution for this problem is the stepping stone to the methodology used in this work and helps ascertain the correct implementation of FEniCS weak formulations, objective function of mean compliance and mean transduction, MMA optimization routine, and mesh-independent filters.

The left and lower boundaries are symmetry axes to reduce the size of the domain

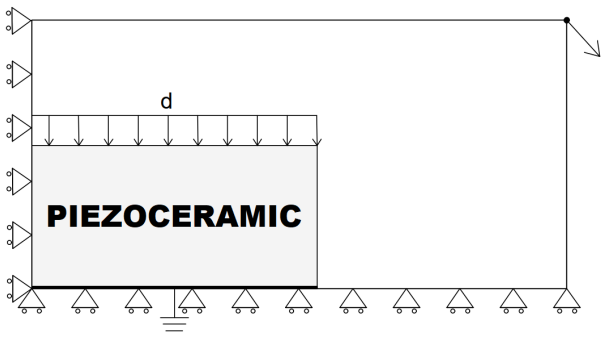

Figure 5.5 – Design specifications of a flextensional actuator (symmetry is applied here).

by three-quarters, they constrict movement on the x and y axes respectively. The arrow on the top right corner represents the desired displacement of the compliant mechanism. The region defined by d is the electrode region with the positive electric potential. The result obtained by the FEniCS implementation is compared to the result presented in Silva et al. [2003] and in Silva et al. [2000]. Table 5.3 presents the materials used in Silva et al. [2000] and for this benchmark.

Dielectric constants are usually expressed as a dimensionless property, being the ratio of the permittivity of the material in relation to 0, the vacuum permittivity. According to NIST, the National Institute of Standards and Technology, ε_0 has a value of approximately $8.854 \times 10^{12} F/m$. Figure 5.6 shows the result obtained in this dissertation together with the ones in the literature. The distinct parts of the topology presented are caused by different materials (in the case of Figure 5.6b) and different filters (in both cases).

The M_{nd} for this problem was 23.303%, showing the presence of a lot of grey area. In the way the problem was constructed, all the piezoelectric material was set to have a pseudo density of 0.5. Ignoring the area of the piezo material, the M_{nd} value becomes 1.871%, a more consolidated value.

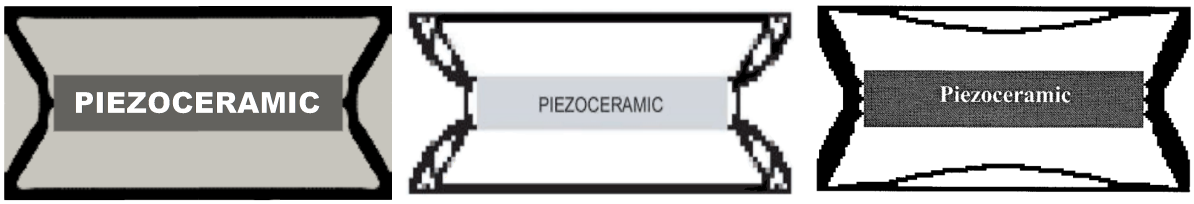

(a) (b) (c)

Figure 5.6 – (a) Obtained design; (b) Actuator f2b0830 [SILVA et al., 2003]; and (c) design obtained by SILVA et al.[2000].

The final design was obtained after 30 iterations on a 10000 elements mesh, with the same element as proposed in the subsection 5.1.1. The final displacement in the output region was 1.64×10^{-8} mm on the horizontal axis and -1.16×10^{-7} mm on the vertical axis, with a 20V electric potential on the upper region of the piezoceramic. The original works of Silva et al. [2000, 2003] are studies of actuators and the information shared is frequency driven. Therefore no static values of displacement were used to quantify the validation

PTZ-5 material properties			
Elastic constants	c_{11}^E	121	GPa
	c_{12}^E	75.4	
	c_{13}^E	75.2	
	c_{33}^E	111	
	c_{44}^E	23	
	c_{66}^E	21	
Piezoelectric constants	e_{31}	-5.4	$\frac{C}{m^2}$
	e_{33}	15.8	
	e_{51}	12.3	
Dielectric constants	$\varepsilon_{11}^S/\varepsilon_0$	1650	–
	$\varepsilon_{33}^S/\varepsilon_0$	1700	
Brass material properties			
Elastic constants	Y	106	GPa
	ν	0.3	–

Table 5.3 – Material properties for the Flextensional problem.

of the compliant mechanism developed. With a qualitative analysis of the topologies and with an output displacement in the correct direction, the benchmark was considered well implemented. With all previous benchmarks working as intended, the next stage was to implement the second variable to optimize the piezoelectric material as well.

5.2 Optimization of a multi-material, piezoelectric activated, compliant mechanism

The aim of this section is to implement the Python code with the capacity to optimize a compliant mechanism activated by piezoelectric material with an electric field, present in section 4.7. Creating an optimization in two levels, optimizing both the piezoelectric material and the isotropic one, evaluating the mechanisms and the displacements achieved. Five distinct problems were created, changing angles of polarization and electric field, symmetries, desirable displacements, and boundary conditions. In the next sections, they will be displayed and discussed.

5.2.1 Problem definition

The first problem explored in this chapter is a 2D optimization, with dimensions of the design domain chosen to be in the millimetric scale to better represent a possible use of this methodology. A square area of 50 by 50 mm with restrain in the y-axis movement of

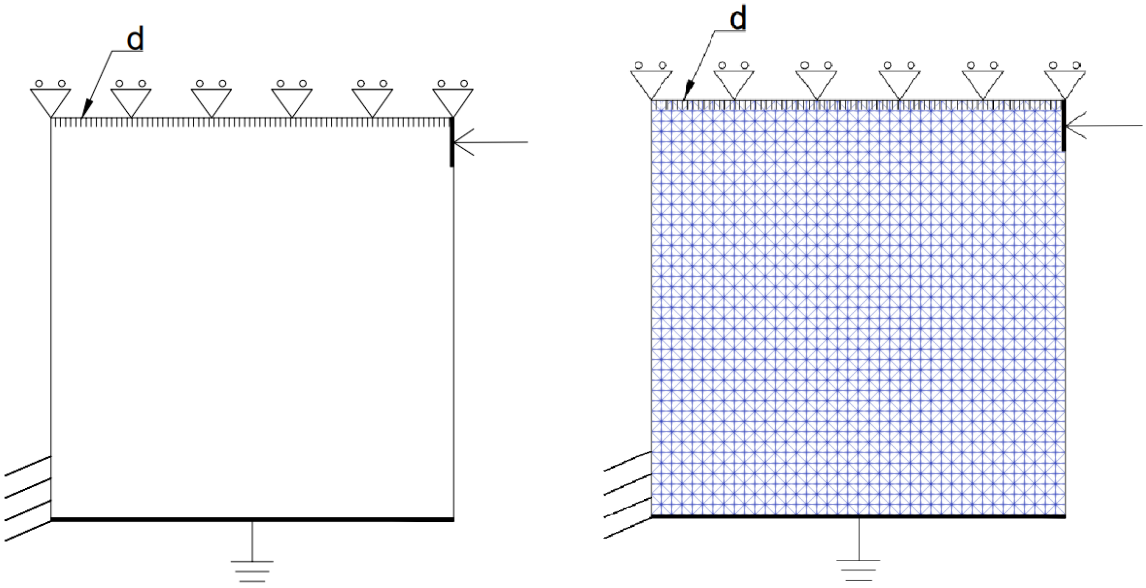

(a) (b)

Figure 5.7 – (a) The design domain with boundary conditions and (b) the mesh model used.

the upper boundary and full restriction of movement on the lower part of the left boundary (5 mm) was selected. The Figure 5.7a shows the domain with all the boundary conditions and the picked objective displacement (a 5mm region) of the compliant mechanism. The small hatched upper region represents an electrode with a prescribed electric potential d, measured in Volts, the bottom border is grounded, creating a vertical electric field. Figure 5.7b shows the final mesh used on the domain. The use of a triangle mesh that stacks in a zigzag pattern is to not have an artificial anisotropy caused by mesh configuration, where one diagonal could have more definition than the other.

The multi-material aspect of the problem means that two distinct materials should be defined. The nonpiezoelectric material picked was an aluminum Al 1050 with mechanical properties listed in table 5.4. The piezoelectric material, PZT-5A, has its properties displayed in the same table. All properties for the piezoceramic are displayed with a polarization on the z-axis, the alterations required to rotate them were explained prior, in chapter 3.2.

To further state the problem, the initial values for the design variables need to be defined. Together with a desirable volume ($\mathfrak{f}_\chi$ and $\mathfrak{f}_\rho$), filter dials, PEMAP weights, and boundary conditions, these values make the overall definition of the proposed problem.

PZT-5A material properties			
Elastic constants	c_{11}^E	121	GPa
	c_{13}^E	75.2	
	c_{33}^E	111	
	c_{66}^E	22.6	
Piezoelectric constants	e_{31}	-5.4	$\frac{C}{m^2}$
	e_{33}	15.8	
	e_{51}	12.3	
Dielectric constants	$\varepsilon_{11}^S/\varepsilon_0$	916	–
	$\varepsilon_{33}^S/\varepsilon_0$	830	
Al 1050 material properties			
Elastic constants	Y	71	GPa
	ν	0.33	–

Table 5.4 – Material properties for the optimization of piezoelectric activated compliant mechanisms.

d[V]	200	α	0.5
$\boldsymbol{t_2}$	[-1,0]	β_0	1
$\boldsymbol{\chi_0}$	**0.5**	β_{max}	128
$\boldsymbol{\rho_0}$	**0.25**	r	0.2
$\mathfrak{f}_\chi$	0.5	η_0, η_1	3
$\mathfrak{f}_\rho$	0.25	η_2	1

Table 5.5 – Initial values for the first problem

Table 5.5 shows these initial conditions. β_0 represents the initial value for the smooth Heaviside function, that after some iterations double and β_{max} a maximum value for this variable. The initial vectors for the design variables were set to be constant throughout the mesh and have the same value as the desirable volume percentage. Since the problem has no outside force, $\boldsymbol{t_3}$ is defined by $\boldsymbol{t_3} = -\boldsymbol{t_2}$ and it is used to calculate the mean compliance, as shown in Equation 4.7.

The final consideration before solving the topology optimization problem is to determine the stop criteria. A maximum number of iterations of 1000 and a element convergence value of 10^{-3} were selected. To calculate the current element convergence value the difference between each variable and its previous iteration is calculated, then the maximum value of this vector is chosen. If this value is lower than the minimum

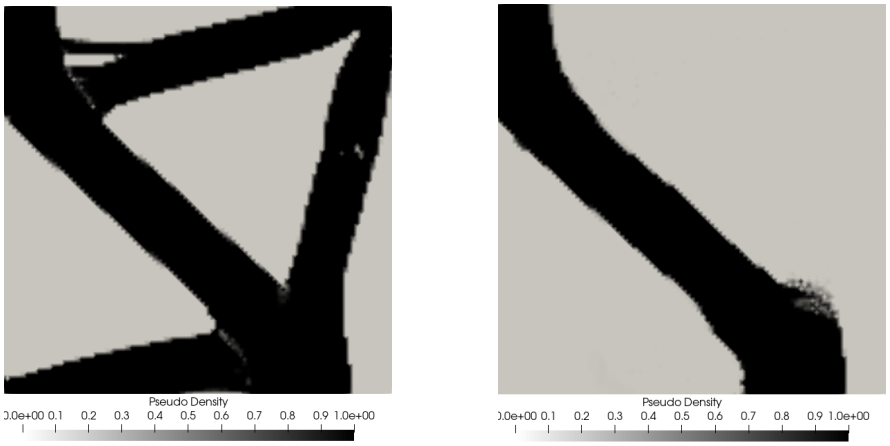

(a) (b)

Figure 5.8 – (a) Final χ distribution; (b) Final ρ distribution.

(10^{-3}), the optimization is considered convergent and the iterations stop, as presented in

$$El_{min} = \min\left(\min\left(\left|\frac{\boldsymbol{\chi}^{[it]} - \boldsymbol{\chi}^{[it-1]}}{\boldsymbol{\chi}^{[it]}}\right|\right), \min\left(\left|\frac{\boldsymbol{\rho}^{[it]} - \boldsymbol{\rho}^{[it-1]}}{\boldsymbol{\rho}^{[it]}}\right|\right)\right) \tag{5.4}$$

where El_{min} is the element convergence value of the current iteration $[it]$.

Another stop criterion was created when the objective function showed signs of convergence but the element convergence was still bigger than 0.1%. The new criterion chosen was the objective convergence, a difference between the objective function of the current iteration and the last. If the last 5 values of objective convergence were smaller than (10^{-3}), the optimization was considered convergent and the program interrupted.

5.2.2 Mesh size

Running the code for a 100x100 mesh grid, the obtained result after 141 iterations is shown in Figure 5.8, representing the values of variables χ and ρ, respectively. On Figure 5.8a, the M_{nd} value was 1.532%, for Figure 5.8b, M_{nd}=0.149%. Both Equations 4.12 and 4.13 are satisfied with χ representing 49.08% of the total design space and ρ representing 24.38%.

Analyzing Figure 5.8, the presence of ρ is visibly dependent on χ, appearing only where the latter has a positive value, instead of zero. This result bears physical meaning since χ is the pseudo density that dictates the absence or the presence of material. If ρ appeared where χ was null, the element would not contribute to the constitutive equa-

Figure 5.9 – Final design for the topology optimized compliant mechanism.

tions shown in Equation 3.9, this restriction occurs naturally in a multi-material problem with two-layer optimization, since with the optimization elements not contributing to the mechanism are discarded. It can also be noticed that the piezoelectric material extends from top to bottom. This is required by the definition of the problem, where the top and bottom regions have prescribed electric potential, without a piezoelectric material running from one border to the other, the gradient E would be discontinued, and therefore no displacement would result from the mechanism.

The final mechanism represented in Figure 5.9 was obtained by colorizing Figures 5.8a and 5.8b with a white-red scale for representing χ and a green-yellow color scale for ρ. Combining both images with ρ on top and excluding any value less then 0.01, the mechanism is presented. The material PZT-5A is present where yellow appears, aluminum is where red is the color, while green tints are the intermediary values between both materials and pinkish tones are representing a mixture of aluminum and void. Figure 5.9 contains a mechanism with some undesirables characteristics. A green region, representing a non binary solution is present in the bottom right part of the mechanism, where both materials would be touching. A small hole on the aluminum region made of one element, in other iterations this hole disappears, showing it was a fluke.

The desirable displacement had an initial value of -7.081×10^{-10}mm and after the optimization, this value was -8.186×10^{-8}mm, still an infinitesimal amount, but two orders of magnitude larger than the initial. The displacement shown in the mechanism can be seen in Figure 5.10, with an increase in the displacement scale for better visualization.

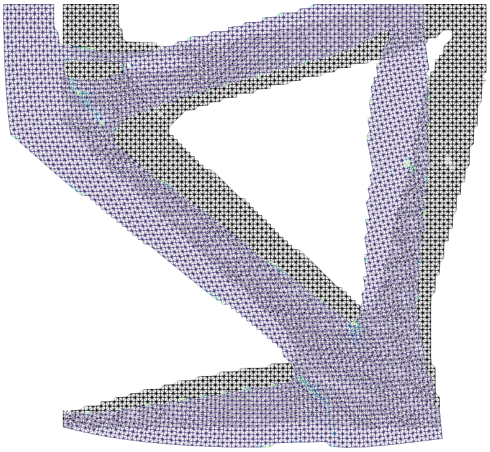

Figure 5.10 – Displacement of the compliant mechanism. In black, the mesh without the electric field, in blue, the mesh with electric field applied.

In black, the mesh without any deformation and in blue, the mesh with the boundary conditions applied.

The results of topology optimizations should be mesh-independent to a certain degree. With a very small number of elements, no real mechanism can be visualized, but with enough resolution, the design should be very similar among distinct mesh sizes. The same is true for the objective function: with minor fluctuations caused by slight numerical changes, the overall behavior of the objective function should be consistent among different mesh sizes. Figure 5.11 shows the values of the objective function in the defined problem for five distinct mesh sizes, 20x20, 40x40, 60x60, 80x80, and 100x100. The scale present on the graph depicted in Figure 5.11 is logarithmic for better visualization, since the initial values are orders of magnitude larger than the subsequent ones.

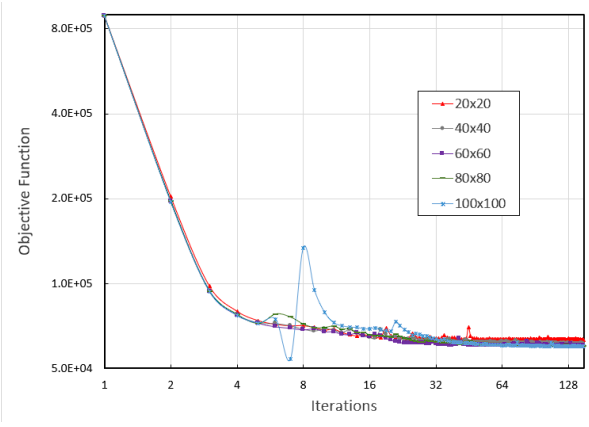

Figure 5.11 – Objective function optimized.

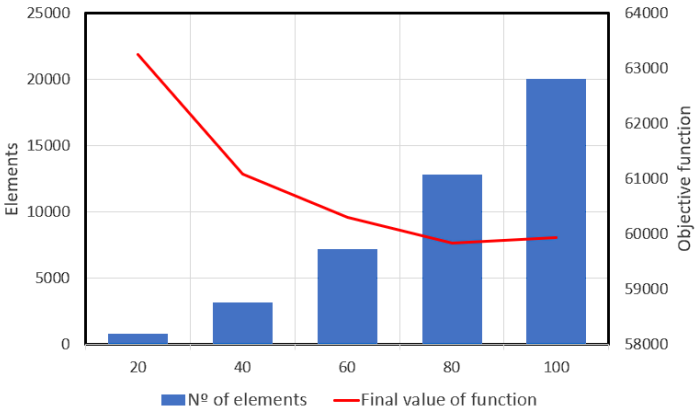

Figure 5.12 – Objective function and mesh resolution.

Analyzing the graph, some fluctuations occur where the value of the objective function changes values drastically, but are quickly returned and the overall behavior of the objective function is the same for every mesh resolution tested. In Figure 5.12, the number of elements and the objective function at 150 iterations are shown. Although all of the problems achieved an objective convergence prior to 150 iterations, to better evaluate the functions, the comparison was made in a fixed iteration. The f_0 values decrease with a more refined mesh but after a big enough resolution the value remains within acceptable tolerance of 10^{-3}.

From Figure 5.12, it can be seen that the best choice of mesh resolution for this particular problem is 80x80. The objective value reached a plateau and the number of elements is significantly lower than the 100x100 mesh, reducing the computational cost. However, only the objective value converging does not guarantee the topology remains the same across mesh variations.

Figure 5.13 shows the topology result of the optimizations for the distinct mesh sizes. It is visible that the overall design remains the same, with more branches appearing in the finer meshes and the contact between materials having the tendency to diminish. The upper contact between the piezoceramic and the aluminum tends to a fractal canopy topology to better transform the y elongation of the piezoelectric material to horizontal displacement. By elongating in the y-axis, the triangle composed of vertical connections between both materials and the branch origin enlongates in the vertical axis while shortening on x-axis

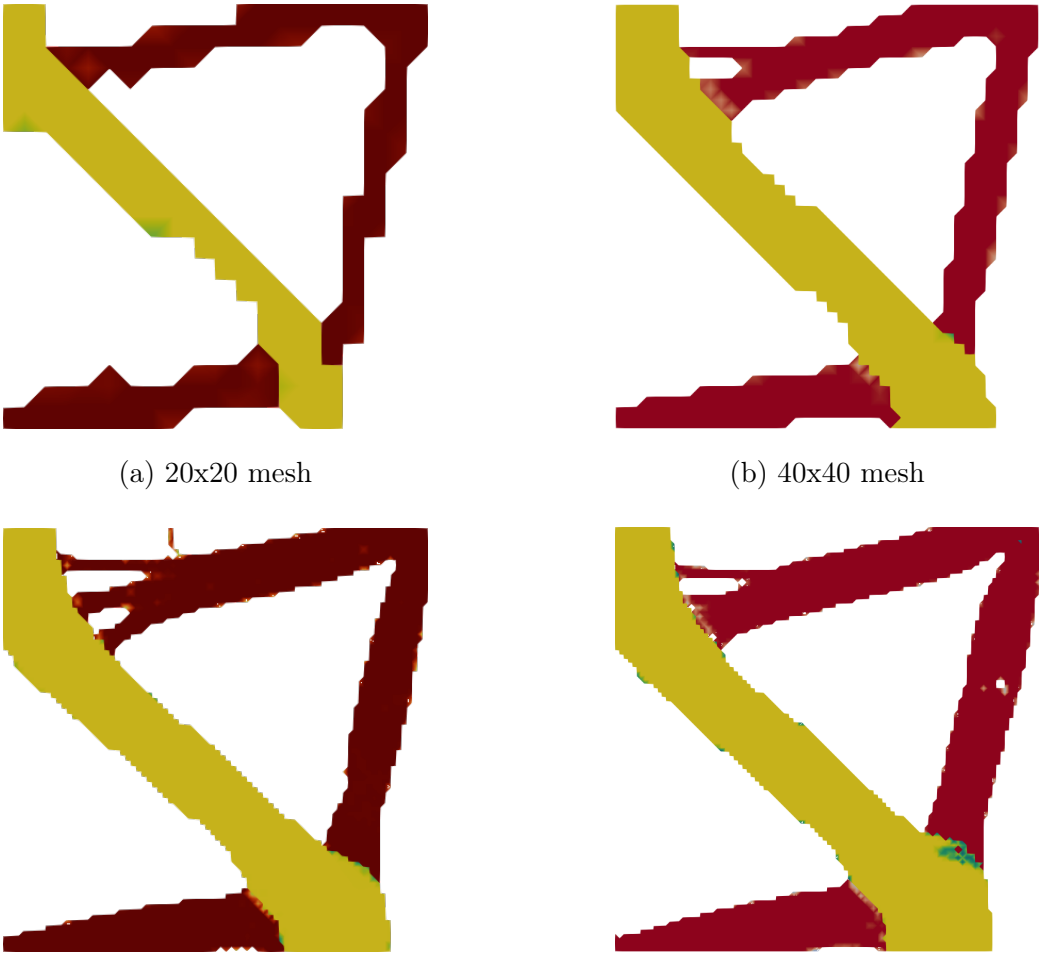

(a) 20x20 mesh

(b) 40x40 mesh

(c) 80x80 mesh

(d) 100x100 mesh

Figure 5.13 – Compliant mechanism for different mesh sizes.

5.3 Additional design problems

To further analyze the results of the implemented code, another four distinct problems were created after the first. The design domains of these optimization problems were chosen to create a large number of distinct features. Table 5.6 exhibits the initial variables of each problem, with all the problems being squares of side 50mm, mesh size 80x80. Some of the problems can be reduced to half by having some axe of symmetry, on those cases the mirror side will have 25mm of length and be 40 cells wide.

The unmentioned values of table 5.6 are equal to all cases and can be seen in table 5.5 with the exception of $\boldsymbol{\chi}_0$ and $\boldsymbol{\rho}_0$ that are defined as vectors with all values equal to $\mathfrak{f}_\chi$ and $\mathfrak{f}_\rho$, respectively.

	$\mathfrak{f}_\chi$	$\mathfrak{f}_\rho$	domain size	θ	$\boldsymbol{t_2}$
(a)	0.5	0.25	25x50 mm	π	[0,1]
(b)	0.4	0.2	50x50 mm	0	[0,-1]
(c)	0.3	0.15	50x25 mm	π	[1,0]
(d)	0.5	0.4	50x50 mm	$\pi/2$	[1,0]

Table 5.6 – Initial values for the additional design problems.

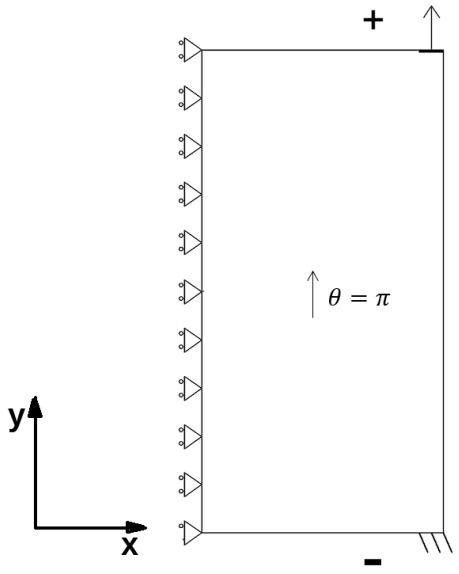

Figure 5.14 – Vertical amplifier problem boundary conditions

5.3.1 Second problem: vertical displacement amplifier

The second problem tested with the methodology described in this work is presented in Figure 5.14. The vertical amplifier aims to maximize the displacement of the right upper corner of the domain. The design domain is a square of size 50mm with vertical symmetric boundary conditions, it can be reduced by half with prescribed displacement on the x-axis of zero in the symmetry axis. With clamped bottom corners, a prescribed electric potential (represented by the + and - signals) of 200V, and a desirable output displacement indicated by the upwards arrow, the problem is fully defined.

With an angle of π between the electric field and the polarization of the piezoelectric material, the initial displacement of PZT-5A is to contract in the y-axis and expand in the abscissa. This deformation is in opposition to the desired output, so the mechanism is not as trivial as it would be if $\theta = 0$. The final mechanism can be seen in Figure 5.15a, with calculated M_{nd} equal to 0.0128 for χ and 0.0317 for ρ.

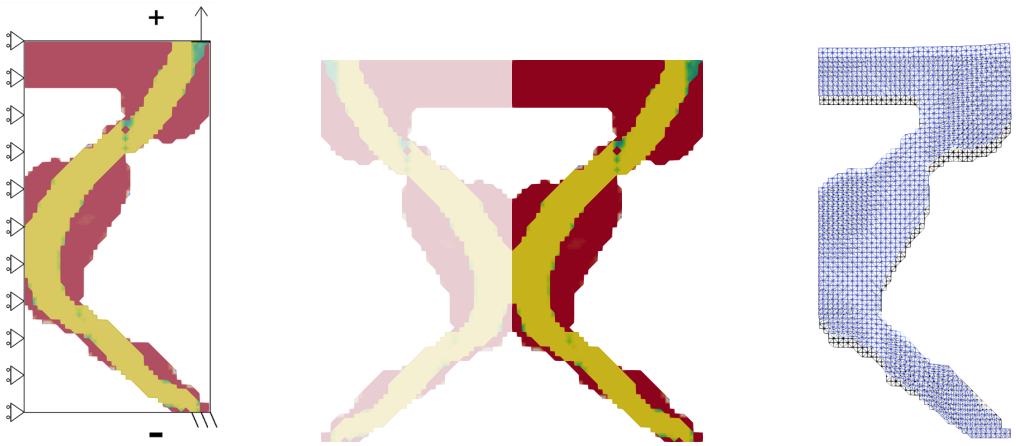

(a) (b) (c)

Figure 5.15 – (a) Compliant mechanism topology for the vertical displacement amplifier, (b) the full device, and (c) the displacement caused by the electric field

As in the previous problem, the piezoceramic bridges top and bottom boundaries. The mechanism uses aluminum to constrict movement in the x-axis and to create a lever on the top region to make the horizontal extension contribute to the objective displacement, represented in the Figure 5.15c. The initial objective function of this problem was calculated to be 62314.79, while at the end of the 78th iteration, the objective function was 2810.14. The achieved displacement on the output region (10% of the length parameter, that is, 2.5 mm) was 7.116×10^{-8} mm.

5.3.2 Third problem: vertical displacement amplifier without imposed symmetry

The third problem developed, similarly to the second one, has a vertical symmetry axis, but no simplification of the design domain was made. This choice had the purpose to inspect if a symmetric compliant mechanism would be created without the imposed symmetry nonetheless. Remaining a square of side 50 mm and with the bottom side fixed, the domain has an output region located in the upper side with length of 5mm. Another change in the design is the electric field on this problem. The prescribed electrodes are on vertical sides, requiring the rotation of the polarized material to remain aligned with the electric field. The constitutive matrices in this problem require similar rotations and changes to the ones used for the benchmark problem of the surface-mounted actuation

beam on Equation 5.3. Figure 5.16 presents the design domain with the boundary conditions.

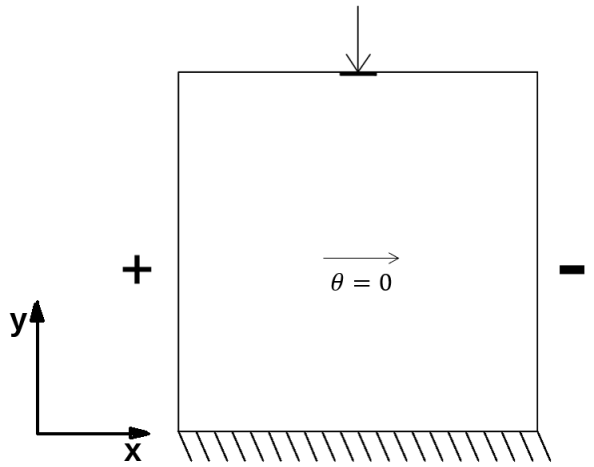

Figure 5.16 – Vertical displacement amplifier problem boundary conditions

Figure 5.17a shows the final topology after 127 iterations. The M_{nd} values for χ and ρ were 0.0121 and 0.0516, respectively. It is possible to see the symmetry arising as it was predicted. The M_{nd} for ρ is 5%, meaning an expressive amount of grey areas (represented with the green tilt in the colorized image). The stop criterion for the program was five iterations with less than 0.1% change in the objective function, showing a plateau. The displacement presented in Figure 5.17b is -4.534×10^{-8} mm, this value is lesser then the other ones present in this dissertation, part of this stands from the use of d31 modulus, where the output is mostly driven by the constriction happening in the y instead of the elongation of x, part because the final device bears a close resemblance to a truss structure. The initial and final objective function values were 298788 and 8130 respectively.

5.3.3 Fourth problem: horizontal displacement amplifier

The next problem developed was created with a horizontal symmetry and two regions of constraint, represented in Figure 5.18, with a displacement-restricted area opposite to the desirable output and on the top of the domain and with size of 50x25 mm^2. The horizontal symmetry can be accomplished in two ways: mirroring all the design constraints appearing in Figure 5.18, including positive and negative electric potentials and polarization angle, meaning the full mechanism would need a boundary condition in the middle of the domain. Or preserving the relationship with an electric field and polar-

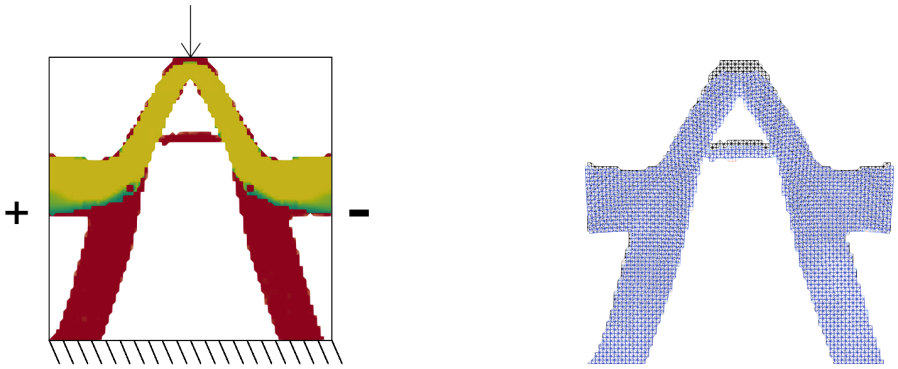

(a) (b)

Figure 5.17 – (a) Compliant mechanism topology for the Vertical displacement amplifier without imposed symmetry and (b) the displacement caused by the electric field

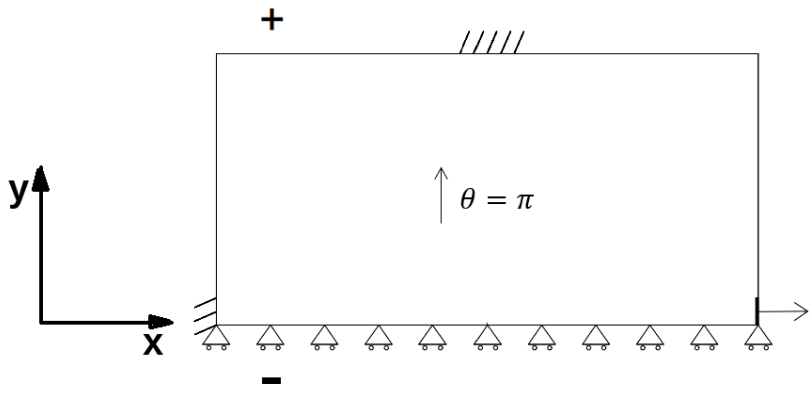

Figure 5.18 – Horizontal displacement amplifier problem boundary conditions

ization of the top half, that is, an angle of π and 200V in 25 mm, and create a bottom one with the same characteristics. In this particular example, the top boundary has an electric potential of 200V while the symmetry axis has 0V. To recreate the same problem with a full domain, while the top electric potential would remain the same, the bottom boundary would have -200V of electric potential, and the entire domain would have a uniform polarization angle of π.

The optimal solution for the piezoelectric compliant mechanism is exhibited in Figure 5.19a. The gray values for χ and ρ were 0.0114 and 0.0112, respectively. The number of iterations required for the objective function to stabilize was 72. As with all problems using this methodology, the piezoelectric material bridged the electric potential boundaries, and the upper boundary was nested in close proximity to the fixed region,

(a) (b) (c)

Figure 5.19 – (a) Compliant mechanism topology for the Horizontal amplifier, (b) the full device, and (c) the displacement caused by the electric field

which was filled with isotropic material. This optimization problem had the polarization in the opposite direction of the electric field and the initial objective function was calculated as 1716573 with the last iteration having a value of 6641. The horizontal displacement of the output region (2.5mm) was 9.310×10^{-8} mm. The constriction on the left was unused by this mechanism, since it hinders the horizontal movement.

5.3.4 Fifth problem: Perpendicular polarization mechanism

The fifth and final example created for this work was the following: a square of 50x50mm with a fixed bottom and an electric potential positive on top and negative on bottom. The mechanism should displace the right corner region (5mm) in the positive x-axis. This problem is presented in Figure 5.20. The distinct characteristic of this problem in regards to all the previous ones is the polarization angle, while the other topologies had aligned polarization with electric field with both orientations, this problem has a perpendicular polarization. As seen in chapter 3.1, the piezoelectric material will shear in a perpendicular electric field. Another distinct characteristic of this particular problem is the heavy amount of piezoceramic in comparison to aluminum.

Figure 5.21a presents the compliant mechanism obtained after 49 iterations of the topology optimization problem, the initial and final values for the optimized function were 56739 and 6663. The χ has 0.6726% of gray area while ρ has 0.6727%. The fast convergence of this problem is due to the low volume fraction of distinct materials, while other compliant mechanisms were made with 50% aluminum and 50% PZT-5A the one in question has 80% piezoceramic and 20% aluminum. The horizontal displacement obtained

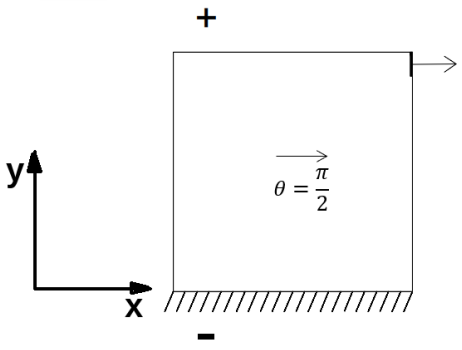

Figure 5.20 – Fifth optimization problem boundary conditions

was 2.259×10^{-7} mm.

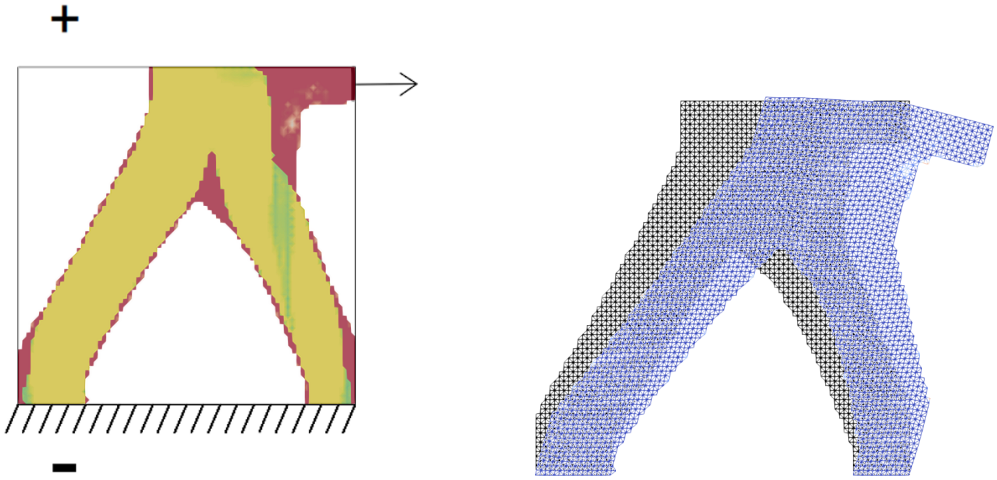

(a) (b)

Figure 5.21 – (a) Compliant mechanism topology for the perpendicular polarization mechanism and (b) the displacement caused by the electric field

6 CONCLUSIONS

A topology optimization of compliant mechanisms activated by piezoceramics was proposed. The piezoelectric phenomenon was explained and quantified through the constitutive equations, the concepts of compliant mechanisms and topology optimization were defined, as well as the concepts for mean transduction and mean compliance. The methodology implemented in this dissertation manages to achieve desirable topologies for both the piezoelectric material and the isotropic nonpiezoelectric material, creating compliant mechanisms capable of increasing the desirable output displacement.

The PEMAP was successfully used to optimize the piezoceramic and the final results show compliant mechanisms in accordance with the design constraints and, utilizing the filters chosen for this work, minimal grey area and checkerboard patterns. The use of in-plane polarization contributes to the study of TO using piezoelectric material, the flexibility of polarization and electric field allows distinct mechanisms using elongation, constriction or sheer deformations to achieve the CM's objective.

The objective of creating a methodology and a Python code capable of solving topology optimizations of compliant mechanisms using electric fields and piezoelectric material as activators was achieved. The free licensing of all tools used for the creation of the code proposed in this dissertation allows for the sharing and building of the main code. The benchmarks proposed to verify the applications envelop the main ideas and implementations of the proposed problem, allowing a step-by-step approach to the optimization. The generic plane stress with an in-plane polarization compliant mechanism topology optimization problem can be solved with the Python codes available at https://github.com/apivar/Dissertation .

6.1 Suggestions for future works

To further the studies on the topics presented in this work, some paths are proposed:

- Implement the PiezoElectric MAterial with Penalization and Polarization (PEMAP-P) methodology, where the polarization direction of the piezoelectric material is fixed but its orientation can be optimized, as previously done by Gonçalves et al. [2019].

- Similarly to optimize the fiber orientation of a composite material, the θ can be made into a design variable, having different polarization regions.

- Evaluate the possibility of using boundary condition propagation to find solutions with design-dependent electrodes. When the piezoelectric material is considered polarized in the direction perpendicular to the plane, it can be assumed that both potential and ground electrodes are defined in the whole domain, as presented in Carbonari et al. [2007]. However, to generate forces in the plane efficiently using piezoelectric material that is also polarized in a direction in the plane, it is required to consider the electrodes as boundary conditions, which makes the design dependent on the electrode configuration. A propagation scheme similar to the one proposed by Moscatelli et al. [2023] could improve the performance of the designed mechanism by applying the electrodes only where the piezoelectric material is defined, according to the optimization progress.

- Implement contact within both materials. Since piezoceramics are very brittle, the regions of contact between the materials can be susceptible to fracture damage.

- Expand the work to dynamic problems. All solutions presented here in this dissertation were static solutions, one of the biggest problems with compliant mechanisms is the fact that they are favorable to fatigue. The use of piezoelectric in vibration problems is also a reason to deepen the knowledge of the topic.

- Create a physical mechanism. Manufacturing a design obtained through the methodology presented in this paper and then evaluating the theoretical displacement and the one obtained with the prototype would help future development on the field.

REFERENCES

Standards on piezoelectric crystals, 1949. *Proceedings of the IRE*, 37(12):1378–1395, 1949. doi: 10.1109/JRPROC.1949.229975.

Mostafa Abdalla, Mary Frecker, Zafer Gürdal, Terrence Johnson, and Douglas K Lindner. Design of a piezoelectric actuator and compliant mechanism combination for maximum energy efficiency. *Smart Materials and Structures*, 14(6):1421–1430, November 2005. doi: 10.1088/0964-1726/14/6/035. URL https://doi.org/10.1088/0964-1726/14/6/035.

Alejandro Eduardo Albanesi, Víctor D. Fachinotti, and Martin Pucheta. A review on design methods for compliant mechanisms. 2010.

Martin S. Alnæs, Anders Logg, Kristian B. Ølgaard, Marie E. Rognes, and Garth N. Wells. Unified form language. *ACM Transactions on Mathematical Software*, 40(2):1–37, February 2014. doi: 10.1145/2566630.

M. S. Alnæs, J. Blechta, J. Hake, J. Johansson, B. Kehlet, A. Logg, C. Richardson, J. Ring, M. E. Rognes, and G. N. Wells. The FEniCS Project Version 1.5. *Archive of Numerical Software*, 3(100):9–23, 2015. doi: 10.11588/ans.2015.100.20553.

Diego Hayashi Alonso. *Topology optimization for 2D swirl flows with application in the design of a ventricular assist device.* PhD thesis. URL https://doi.org/10.11606/t.3.2022.tde-07072022-094033.

Erik Andreassen, Anders Clausen, Mattias Schevenels, Boyan S. Lazarov, and Ole Sigmund. Efficient topology optimization in MATLAB using 88 lines of code. *Structural and Multidisciplinary Optimization*, 43(1):1–16, November 2010. doi: 10.1007/s00158-010-0594-7. URL https://doi.org/10.1007/s00158-010-0594-7.

Miguel Tobias Bahia. *Otimização topológica aplicada ao projeto de mecanismos flexíveis.* masters dissertation, Universidade Federal de Santa Catarina, 2005.

Martin Philip Bendsøe and Noboru Kikuchi. Generating optimal topologies in structural design using a homogenization method. *Computer Methods in Applied Mechanics and Engineering*, 71(2):197–224, 1988. ISSN 0045-7825. doi: https://doi.org/10.1016/0045-7825(88)90086-2.

Martin Philip Bendsøe and Ole Sigmund. *Topology Optimization: Theory, Methods and Applications.* Springer, February 2004. ISBN 9783540429920.

Ronny C Carbonari, Emílio C N Silva, and Shinji Nishiwaki. Optimum placement of piezoelectric material in piezoactuator design. *Smart Materials and Structures*, 16(1):207–220, jan 2007. doi: 10.1088/0964-1726/16/1/025.

Ronny Calixto Carbonari. *Projeto de atuadores piezelétricos flextensionais usando o método de otimização topológica.* PhD thesis, 2003. URL https://doi.org/10.11606/d.3.2003.tde-08082003-124007.

Enrique Castillo, Roberto Mínguez, and Carmen Castillo. Sensitivity analysis in optimization and reliability problems. *Reliability Engineering &amp System Safety*, 93 (12):1788–1800, December 2008. doi: 10.1016/j.ress.2008.03.010. URL https://doi.org/10.1016/j.ress.2008.03.010.

Stephen C. Cowin. Properties of the anisotropic Elasticity tensor. *The Quarterly Journal of Mechanics and Applied Mathematics*, 42(2):249–266, 1989. doi: 10.1093/qjmam/42.2.249. URL https://doi.org/10.1093/qjmam/42.2.249.

Jacques Curie and Pierre Curie. Développement par compression de l'électricité polaire dans les cristaux hémièdres à faces inclinées. *Bulletin de Minéralogie*, 3(4):90–93, 1880. doi: 10.3406/bulmi.1880.1564. URL https://www.persee.fr/doc/bulmi_0150-9640_1880_num_3_4_1564.

Timothy A. Davis. *UMFPACK User Guide*. Dept. of Computer and Information Science and Engineering Univ. of Florida, Gainesville, FL.

Jacqueline de Miranda Kian. *Topology optimization method applied to design channels considering non-newtonian fluid flow.* PhD thesis. URL https://doi.org/10.11606/d.3.2018.tde-05012018-084558.

Arjen Deetman. Mma.py. URL https://github.com/arjendeetman/GCMMA-MMA-Python.

A. Díaz and O. Sigmund. Checkerboard patterns in layout optimization. *Structural Optimization*, 10(1):40–45, August 1995. doi: 10.1007/bf01743693. URL https://doi.org/10.1007/bf01743693.

Mohamed Fanni, N. Shabara, and Mohamed Alkalla. A comparison between different topology optimization methods. *Engineering Journal*, 38, 12 2013.

M. I. Frecker, G. K. Ananthasuresh, S. Nishiwaki, N. Kikuchi, and S. Kota. Topological synthesis of compliant mechanisms using multi-criteria optimization. *Journal of Mechanical Design*, 119(2):238–245, June 1997. doi: 10.1115/1.2826242. URL https://doi.org/10.1115/1.2826242.

Wenjie Ge and Xin Kou. Topology optimization of multi-materials compliant mechanisms. *Applied Sciences*, 11(9):3828, April 2021. doi: 10.3390/app11093828. URL https://doi.org/10.3390/app11093828.

Juliano F. Gonçalves, Daniel M. De Leon, and Eduardo A. Perondi. Simultaneous optimization of piezoelectric actuator topology and polarization. *Structural and Multidisciplinary Optimization*, 58(3):1139–1154, mar 2018. doi: 10.1007/s00158-018-1957-8.

Juliano Fagundes Gonçalves, Daniel Milbrath De Leon, and Eduardo André Perondi. A simultaneous approach for compliance minimization and piezoelectric actuator design considering the polarization profile. *International Journal for Numerical Methods in Engineering*, 121(2):334–353, October 2019. doi: 10.1002/nme.6211. URL https://doi.org/10.1002/nme.6211.

Juliano Fagundes Gonçalves. *Otimização topológica para localização de atuadores piezelétricos utilizando gramiano de controlabilidade.* masters dissertation, Universidade Federal do Rio Grande do Sul, 2015.

Juliano Fagundes Gonçalves. *Projeto de estruturas inteligentes para controle de vibrações utilizando o método de otimização topológica*. doctoral thesis, Universidade Federal do Rio Grande do Sul, 2019.

James K. Guest, Alireza Asadpoure, and Seung-Hyun Ha. Eliminating beta-continuation from heaviside projection and density filter algorithms. *Structural and Multidisciplinary Optimization*, 44(4):443–453, July 2011. doi: 10.1007/s00158-011-0676-1.

Charles R. Harris, K. Jarrod Millman, Stéfan J. van der Walt, Ralf Gommers, Pauli Virtanen, David Cournapeau, Eric Wieser, Julian Taylor, Sebastian Berg, Nathaniel J. Smith, Robert Kern, Matti Picus, Stephan Hoyer, Marten H. van Kerkwijk, Matthew Brett, Allan Haldane, Jaime Fernández del Río, Mark Wiebe, Pearu Peterson, Pierre Gérard-Marchant, Kevin Sheppard, Tyler Reddy, Warren Weckesser, Hameer Abbasi, Christoph Gohlke, and Travis E. Oliphant. Array programming with NumPy. *Nature*, 585(7825):357–362, September 2020. doi: 10.1038/s41586-020-2649-2.

Meng He, Xiaopeng Zhang, Lucas dos Santos Fernandez, Alexandre Molter, Liang Xia, and Tielin Shi. Multi-material topology optimization of piezoelectric composite structures for energy harvesting. *Composite Structures*, 265:113783, June 2021. doi: 10.1016/j.compstruct.2021.113783.

Larry L. Howell. *Compliant mechanisms*. John Wiley and Sons, 2001.

IEEE. Ieee standard on piezoelectricity. *ANSI/IEEE Std 176-1987*, 1988. doi: 10.1109/IEEESTD.1988.79638.

Carlos De Marqui Junior, Alper Erturk, and Daniel J. Inman. An electromechanical finite element model for piezoelectric energy harvester plates. *Journal of Sound and Vibration*, 327(1-2):9–25, October 2009. doi: 10.1016/j.jsv.2009.05.015. URL `https://doi.org/10.1016/j.jsv.2009.05.015`.

Martin Kögl and Emílio C N Silva. Topology optimization of smart structures: design of piezoelectric plate and shell actuators. *Smart Materials and Structures*, 14(2): 387–399, March 2005. doi: 10.1088/0964-1726/14/2/013.

Gih Keong Lau, Hejun Du, Ningqun Guo, and Mong King Lim. Systematic design of displacement-amplifying mechanisms for piezoelectric stacked actuators using topology optimization. *Journal of Intelligent Material Systems and Structures*, 11(9):685–695, September 2000. doi: 10.1106/17v9-dr0q-6bmu-rkuy.

G.K. Lau, H. Du, and M.K. Lim. Use of functional specifications as objective functions in topological optimization of compliant mechanism. *Computer Methods in Applied Mechanics and Engineering*, 190(34):4421–4433, May 2001. doi: 10.1016/s0045-7825(00)00325-x. URL `https://doi.org/10.1016/s0045-7825(00)00325-x`.

B. S. Lazarov and O. Sigmund. Filters in topology optimization based on helmholtz-type differential equations. *International Journal for Numerical Methods in Engineering*, 86(6):765–781, December 2010. doi: 10.1002/nme.3072.

Daniel M. De Leon, Joe Alexandersen, Jun S. O. Fonseca, and Ole Sigmund. Stress-constrained topology optimization for compliant mechanism design. *Structural and Multidisciplinary Optimization*, 52(5):929–943, July 2015. doi: 10.1007/s00158-015-1279-z.

Daniel M. De Leon, Juliano F. Gonçalves, and Carlos E. de Souza. Stress-based topology optimization of compliant mechanisms design using geometrical and material nonlinearities. *Structural and Multidisciplinary Optimization*, 62(1):231–248, March 2020. doi: 10.1007/s00158-019-02484-4.

R. Lerch. Simulation of piezoelectric devices by two- and three-dimensional finite elements. *IEEE Transactions on Ultrasonics, Ferroelectrics, and Frequency Control*, 37 (3):233–247, 1990. doi: 10.1109/58.55314.

Jiangzi Lin, Liyong Tong, and Zhen Luo. Design and testing of an active core for sandwich panels. Technical report, Sydney Univ (Australia) Dept Of Aeronautical Engineering, 2008.

Gabriel Lippmann. Principe de la conservation de l'électricité, ou second principe de la théorie des phénomènes électriques. *Journal of Physics: Theories and Applications*, 10(1):381–394, 1881.

Liying Liu, Jian Xing, Qingwei Yang, and Yangjun Luo. Design of large-displacement compliant mechanisms by topology optimization incorporating modified additive hyperelasticity technique. *Mathematical Problems in Engineering*, 2017:1–11, 2017. doi: 10.1155/2017/4679746. URL `https://doi.org/10.1155/2017/4679746`.

Tingyu Liu, Jun Chen, and Feinan Yan. Optical polarized properties related to the oxygen vacancy in the CaMoO4 crystal. *Journal of Luminescence*, 129(2):101–104, February 2009. doi: 10.1016/j.jlumin.2008.09.007. URL `https://doi.org/10.1016/j.jlumin.2008.09.007`.

Anders Logg, Kent-Andre Mardal, Garth N. Wells, et al. *Automated Solution of Differential Equations by the Finite Element Method*. Springer, 2012. ISBN 978-3-642-23098-1. doi: 10.1007/978-3-642-23099-8.

Jianan Lu and Yonghua Chen. Topology optimization of a prosthetic knee joint component. In *2010 International Conference on Manufacturing Automation*. IEEE, December 2010. doi: 10.1109/icma.2010.52. URL `https://doi.org/10.1109/icma.2010.52`.

Zhen Luo, Wei Gao, and Chongmin Song. Design of multi-phase piezoelectric actuators. *Journal of Intelligent Material Systems and Structures*, 21(18):1851–1865, November 2010. doi: 10.1177/1045389x10389345. URL `https://doi.org/10.1177/1045389x10389345`.

Yoichi Mamiya. Applications of piezoelectric actuator. *Nec Technical Journal*, 1: 82–86, 2006.

Kurt Maute and Dan M. Frangopol. Reliability-based design of MEMS mechanisms by topology optimization. *Computers &amp Structures*, 81(8-11):813–824, May 2003. doi: 10.1016/s0045-7949(03)00008-7. URL `https://doi.org/10.1016/s0045-7949(03)00008-7`.

Sebastian Mitusch, Simon Funke, and Jørgen Dokken. dolfin-adjoint 2018.1: automated adjoints for FEniCS and firedrake. *Journal of Open Source Software*, 4(38):1292, June 2019. doi: 10.21105/joss.01292.

S. Moheimani and Andrew Fleming. *Piezoelectric Transducers for Vibration Control and Damping*. Springer-Verlag, 01 2006. ISBN 978-1-84628-331-4. doi: 10.1007/1-84628-332-9.

Alexandre Molter, Jun Sérgio Ono Fonseca, and Lucas dos Santos Fernandez. Simultaneous topology optimization of structure and piezoelectric actuators distribution. *Applied Mathematical Modelling*, 40(9-10):5576–5588, May 2016. doi: 10.1016/j.apm.2016.01.023. URL https://doi.org/10.1016/j.apm.2016.01.023.

Jean-Paul Montagner. Upper mantle anisotropy from surface wave studies. *Treatise on Geophysics- Volume 1- Seismology and Structure of the Earth*, 2008.

Marco Montemurro, Thibaut Rodriguez, Jérôme Pailhès, and Paul Le Texier. On multi-material topology optimisation problems under inhomogeneous neumann–dirichlet boundary conditions. *Finite Elements in Analysis and Design*, 214:103867, February 2023. doi: 10.1016/j.finel.2022.103867. URL https://doi.org/10.1016/j.finel.2022.103867.

Eduardo Moscatelli. *Design of pneumatic and hydraulic soft actuators by topology optimization method.* PhD thesis, 2020. URL https://doi.org/10.11606/d.3.2020.tde-21102020-111748.

Eduardo Moscatelli, Luís F.N. Sá, Hélio Emmendoerfer, and Emílio C.N. Silva. Pure-displacement formulation and bulk modulus propagation for topology optimization with pressure loads. *Computer Methods in Applied Mechanics and Engineering*, 411: 116058, June 2023. doi: 10.1016/j.cma.2023.116058. URL https://doi.org/10.1016/j.cma.2023.116058.

Shinji Nishiwaki, Mary I. Frecker, Seungjae Min, and Noboru Kikuchi. Topology optimization of compliant mechanisms using the homogenization method. *International Journal for Numerical Methods in Engineering*, 42(3):535–559, June 1998. doi: 10.1002/(sici)1097-0207(19980615)42:3<535::aid-nme372>3.0.co;2-j.

Jaejong Park and Alok Sutradhar. A multi-resolution method for 3d multi-material topology optimization. *Computer Methods in Applied Mechanics and Engineering*, 285: 571–586, March 2015. doi: 10.1016/j.cma.2014.10.011. URL https://doi.org/10.1016/j.cma.2014.10.011.

Vincent Piefort. *Finite element modelling of piezoelectric active structures.* PhD thesis, Université libre de Bruxelles, Faculté des sciences appliquées, 2001.

R.-E. Plessix. A review of the adjoint-state method for computing the gradient of a functional with geophysical applications. *Geophysical Journal International*, 167(2): 495–503, November 2006. doi: 10.1111/j.1365-246x.2006.02978.x. URL https://doi.org/10.1111/j.1365-246x.2006.02978.x.

Anand Ramani. Multi-material topology optimization with strength constraints. *Structural and Multidisciplinary Optimization*, 43(5):597–615, November 2010. doi: 10.1007/s00158-010-0581-z. URL https://doi.org/10.1007/s00158-010-0581-z.

Li Ren, Rui Yang, Dahai Mi, and Dongming Guo. Topology optimization design for micro compliant mechanism with two materials. In Yunlong Wei, Kil To Chong, Takayuki Takahashi, Shengping Liu, Zushu Li, Zhongwei Jiang, and Jin Young Choi, editors, *SPIE Proceedings*. SPIE, December 2005. doi: 10.1117/12.664803. URL https://doi.org/10.1117/12.664803.

Stephen Roper, Daozhong Li, Vlad Florea, Christopher Woischwill, and Il Yong Kim. Multi-material topology optimization: A practical approach and application. In *SAE Technical Paper Series*. SAE International, April 2018. doi: 10.4271/2018-01-0110. URL https://doi.org/10.4271/2018-01-0110.

George Rozvany and N. Olhoff. *Topology Optimization of Structures and Composite Continua*. Springer, 1st edition, 2000.

D. Ruiz, J. C. Bellido, A. Donoso, and J. L. Sánchez-Rojas. Design of in-plane piezoelectric sensors for static response by simultaneously optimizing the host structure and the electrode profile. *Structural and Multidisciplinary Optimization*, 48(5):1023–1026, April 2013. doi: 10.1007/s00158-013-0923-8. URL https://doi.org/10.1007/s00158-013-0923-8.

B. A. Salamon and A. Midha. An introduction to mechanical advantage in compliant mechanisms. *Journal of Mechanical Design*, 120(2):311–315, June 1998. doi: 10.1115/1.2826974.

Rajat Saxena and Anupam Saxena. On honeycomb parameterization for topology optimization of compliant mechanisms. In *Volume 2: 29th Design Automation Conference, Parts A and B*. ASMEDC, January 2003. doi: 10.1115/detc2003/dac-48806. URL https://doi.org/10.1115/detc2003/dac-48806.

O. Sigmund. Design of multiphysics actuators using topology optimization – part II: Two-material structures. *Computer Methods in Applied Mechanics and Engineering*, 190(49-50):6605–6627, October 2001a. doi: 10.1016/s0045-7825(01)00252-3.

O. Sigmund. Design of multiphysics actuators using topology optimization – part i: One-material structures. *Computer Methods in Applied Mechanics and Engineering*, 190(49-50):6577–6604, October 2001b. doi: 10.1016/s0045-7825(01)00251-1. URL https://doi.org/10.1016/s0045-7825(01)00251-1.

O. Sigmund and J. Petersson. Numerical instabilities in topology optimization: A survey on procedures dealing with checkerboards, mesh-dependencies and local minima. *Structural Optimization*, 16(1):68–75, August 1998. doi: 10.1007/bf01214002. URL https://doi.org/10.1007/bf01214002.

O Sigmund and S Torquato. Design of smart composite materials using topology optimization. *Smart Materials and Structures*, 8(3):365–379, January 1999. doi: 10.1088/0964-1726/8/3/308.

O. Sigmund, S. Torquato, and I. A. Aksay. On the design of 1–3 piezocomposites using topology optimization. *Journal of Materials Research*, 13(4):1038–1048, April 1998. doi: 10.1557/jmr.1998.0145.

Ole Sigmund. On the design of compliant mechanisms using topology optimization. *Mechanics of Structures and Machines*, 25(4):493–524, 1997. doi: 10.1080/08905459708945415.

Ole Sigmund. Morphology-based black and white filters for topology optimization. *Structural and Multidisciplinary Optimization*, 33(4-5):401–424, January 2007. doi: 10.1007/s00158-006-0087-x. URL https://doi.org/10.1007/s00158-006-0087-x.

Ole Sigmund and Kurt Maute. Topology optimization approaches. *Structural and Multidisciplinary Optimization*, 48(6):1031–1055, August 2013. doi: 10.1007/s00158-013-0978-6.

E. C. Nelli Silva, Shinji Nishiwaki, and Noboru Kikuchi. Design of piezocomposite materials and piezoelectric transducers using topology optimization—part II. *Archives of Computational Methods in Engineering*, 6(3):191–215, September 1999a. doi: 10.1007/bf02896423.

E.C.N. Silva, S. Nishiwaki, and N. Kikuchi. Topology optimization design of flextensional actuators. *IEEE Transactions on Ultrasonics, Ferroelectrics and Frequency Control*, 47(3):657–671, May 2000. doi: 10.1109/58.842054.

Emílio C. Nelli Silva. Apostila pmr 5215 – otimização aplicada ao projeto de sistemas mecânicos, 2007.

Emílio C. Nelli Silva, Shinji Nishiwaki, Jun S. Ono Fonseca, and Noboru Kikuchi. Optimization methods applied to material and flextensional actuator design using the homogenization method. *Computer Methods in Applied Mechanics and Engineering*, 172 (1-4):241–271, April 1999b. doi: 10.1016/s0045-7825(98)00231-x.

Emílio Carlos Nelli Silva and Noboru Kikuchi. Design of piezoelectric transducers using topology optimization. *Smart Materials and Structures*, 8:350–364, 1999. doi: 10.1088/0964-1726/8/3/307.

Emílio Carlos Nelli Silva, Gilder Nader, Alessandro Barbosa Shirahige, and Julio Cezar Adamowski. Characterization of novel flextensional actuators designed by using topology optimization method. *Journal of Intelligent Material Systems and Structures*, 14(4-5):297–308, April 2003. doi: 10.1177/1045389x03034683.

Krister Svanberg. Gcmma-mma. URL https://www.smoptit.se/.

Krister Svanberg. The method of moving asymptotes—a new method for structural optimization. *International Journal for Numerical Methods in Engineering*, 24(2):359–373, 1987. doi: https://doi.org/10.1002/nme.1620240207.

Yu-Chong Tai. Introduction to MEMS. In *Microsystems and Nanotechnology*, pages 187–206. Springer Berlin Heidelberg, 2012. doi: 10.1007/978-3-642-18293-8_6.

Masao Tanaka, Masahiro Todoh, and Akihisa Naomi. Adaptive stiffness design for multimaterial structural system. *Journal of Intelligent Material Systems and Structures*, 14(4-5):323–329, April 2003. doi: 10.1177/1045389x03036214. URL https://doi.org/10.1177/1045389x03036214.

H.F. Tiersten. Hamilton's principle for linear piezoelectric media. *Proceedings of the IEEE*, 55(8):1523–1524, 1967. doi: 10.1109/PROC.1967.5887.

Bo Wang, Yan Zhou, Yiming Zhou, Shengli Xu, and Bin Niu. Diverse competitive design for topology optimization. *Structural and Multidisciplinary Optimization*, 57(2): 891–902, August 2017. doi: 10.1007/s00158-017-1762-9. URL https://doi.org/10.1007/s00158-017-1762-9.

Michael Yu Wang. Mechanical and geometric advantages in compliant mechanism optimization. *Frontiers of Mechanical Engineering in China*, May 2009. doi: 10.1007/s11465-009-0066-1. URL https://doi.org/10.1007/s11465-009-0066-1.

L. Yin and G.K. Ananthasuresh. Topology optimization of compliant mechanisms with multiple materials using a peak function material interpolation scheme. *Structural and Multidisciplinary Optimization*, 23(1):49–62, December 2001. doi: 10.1007/s00158-001-0165-z. URL https://doi.org/10.1007/s00158-001-0165-z.

Daoyuan Yu, Shouyu Cai, Tong Gao, and Weihong Zhang. A 168-line MATLAB code for topology optimization with the adaptive bubble method (ABM). *Structural and Multidisciplinary Optimization*, 66(1), December 2022. doi: 10.1007/s00158-022-03403-w. URL https://doi.org/10.1007/s00158-022-03403-w.

X D Zhang and C T Sun. Formulation of an adaptive sandwich beam. *Smart Materials and Structures*, 5(6):814–823, December 1996. doi: 10.1088/0964-1726/5/6/012. URL https://doi.org/10.1088/0964-1726/5/6/012.

Bin Zheng, Ching-Jui Chang, and Hae Chang Gea. Topology optimization of energy harvesting devices using piezoelectric materials. *Structural and Multidisciplinary Optimization*, 38(1):17–23, May 2008. doi: 10.1007/s00158-008-0265-0.

M. Zhou, Y.K. Shyy, and H.L. Thomas. Checkerboard and minimum member size control in topology optimization. *Structural and Multidisciplinary Optimization*, 21(2): 152–158, April 2001. doi: 10.1007/s001580050179. URL https://doi.org/10.1007/s001580050179.

Benliang Zhu, Xianmin Zhang, Hongchuan Zhang, Junwen Liang, Haoyan Zang, Hai Li, and Rixin Wang. Design of compliant mechanisms using continuum topology optimization: A review. *Mechanism and Machine Theory*, 143:103622, 2020. ISSN 0094-114X. doi: https://doi.org/10.1016/j.mechmachtheory.2019.103622.

Wenjie Zuo and Kazuhiro Saitou. Multi-material topology optimization using ordered SIMP interpolation. *Structural and Multidisciplinary Optimization*, 55(2):477–491, June 2016. doi: 10.1007/s00158-016-1513-3.